HHS Public Access

Author manuscript

Cell Rep. Author manuscript; available in PMC 2019 April 26.

Published in final edited form as:

Cell Rep. 2019 April 09; 27(2): 549–560.e6. doi:10.1016/j.celrep.2018.12.055.

TRIM9-Mediated Resolution of Neuroinflammation Confers Neuroprotectionupon Ischemic Stroke in Mice

Jianxiong Zeng[1,9], **Yaoming Wang**[2,3,9], **Zhifei Luo**[4], **Lin-Chun Chang**[1], **Ji Seung Yoo**[1], **Huan Yan**[1], **Younho Choi**[1], **Xiaochun Xie**[2,3], **Benjamin E. Deverman**[5], **Viviana Gradinaru**[5], **Stephanie L. Gupton**[6,7,8], **Berislav V. Zlokovic**[2,3,*], **Zhen Zhao**[2,3,*], and **Jae U. Jung**[1,3,10,*]

[1]Department of Molecular Microbiology and Immunology, Keck School of Medicine, University of Southern California, Los Angeles, CA 90033, USA

[2]Department of Physiology and Neuroscience, Keck School of Medicine, University of Southern California, Los Angeles, CA 90033, USA

[3]Zilkha Neurogenetic Institute, Keck School of Medicine, University of Southern California, Los Angeles, CA 90033, USA

[4]Department of Biochemistry and Molecular Medicine, Keck School of Medicine, University of Southern California, Los Angeles, CA 90033, USA

[5]Division of Biology and Biological Engineering, California Institute of Technology, Pasadena, CA 91125, USA

[6]Neuroscience Center and Curriculum in Neurobiology, University of North Carolina at Chapel Hill, Chapel Hill, NC 27599, USA

[7]Department of Cell Biology and Physiology, University of North Carolina at Chapel Hill, Chapel Hill, NC 27599, USA

[8]Lineberger Comprehensive Cancer Center, University of North Carolina at Chapel Hill, Chapel Hill, NC 27599, USA

[9]These authors contributed equally

[10]Lead Contact

SUMMARY

Excessive and unresolved neuroinflammation is a key component of the pathological cascade in brain injuries such as ischemic stroke. Here, we report that TRIM9, a brain-specific tripartite motif

*Correspondence: zlokovic@usc.edu (B.V.Z.), zzhao@usc.edu (Z.Z.), jaeujung@med.usc.edu (J.U.J.).

AUTHOR CONTRIBUTIONS

J.Z., Z.Z., and J.U.J. designed all experiments, analyzed data, and wrote the paper; J.Z., Y.W., and Z.L. performed experiments and analyzed data, and L.-C.C., J.S.Y., H.Y., Y.C., and X.X. performed experiments. B.E.D., V.G., S.L.G., and B.V.Z. contributed key materials, provided guidance for some experiments, and edited the paper.

SUPPLEMENTAL INFORMATION

Supplemental Information can be found online at https://doi.org/10.1016/j.celrep.2018.12.055.

DECLARATION OF INTERESTS

The authors declare no competing interests.

(TRIM) protein, was highly expressed in the peri-infarct areas shortly after ischemic insults in mice, but expression was decreased in aged mice, which are known to have increased neuroinflammation after stroke. Mechanistically, TRIM9 sequestered β-transducin repeat-containing protein (β-TrCP) from the Skp-Cullin-F-box ubiquitin ligase complex, blocking IκBα degradation and thereby dampening nuclear factor κB (NF-κB)-dependent proinflammatory mediator production and immune cell infiltration to limit neuroinflammation. Consequently, *Trim9*-deficient mice were highly vulnerable to ischemia, manifesting uncontrolled neuroinflammation and exacerbated neuropathological outcomes. Systemic administration of a recombinant TRIM9 adeno-associated virus that drove brain-wide TRIM9 expression effectively resolved neuroinflammation and alleviated neuronal death, especially in aged mice. These findings reveal that TRIM9 is essential for resolving NF-κB-dependent neuroinflammation to promote recovery and repair after brain injury and may represent an attractive therapeutic target.

Graphical Abstract

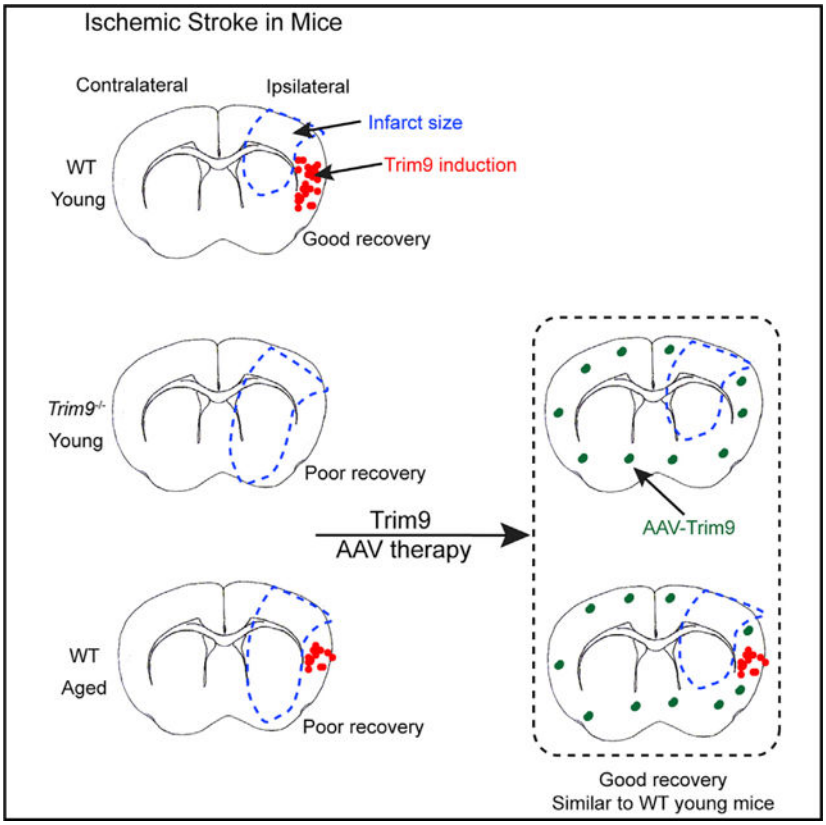

In Brief

Neuroinflammation drives pathology during brain injury. Zeng et al. show that TRIM9 is induced after ischemic insults in young mice, but not old mice, and promotes resolution of neuroinflammation. AAV-mediated TRIM9 therapy in aged mice restricts neuroinflammation and alleviates stroke damage, representing a potential therapeutic target for brain injury.

INTRODUCTION

Tripartite motif containing 9 (TRIM9), a brain-specific ubiquitin (Ub) ligase, is primarily expressed in neurons and regulates netrin-dependent axon guidance and morphogenesis through the interaction with vasodilator-stimulated phosphoprotein (VASP), a mechanism conserved between different species (Hao et al., 2010; Menon et al., 2015; Plooster et al., 2017; Winkle et al., 2016a, 2016c). We have shown that TRIM9 is a potent inhibitor of nuclear factor κB (NF-κB) signaling pathway in *in vitro* cell culture upon cytokine stimulation (Shi et al., 2014). However, the *in vivo* role of TRIM9 in NF-κB-mediated neuroinflammation remains elusive.

Ischemic stroke remains a leading cause of mortality and disabilities in the elderly (Benjamin et al., 2017). Excitotoxicity, oxidative and nitrosative stress, necrosis, and inflammation are key pathogenic events that contribute to neuronal injury and cell death after ischemic stroke (Chamorro et al., 2016; Lo et al., 2005). NF-κB is a master regulator of hypoxia-induced inflammation (Eltzschig and Carmeliet, 2011) and plays important roles in neuronal plasticity, aging, and degeneration in CNS diseases (Gabuzda and Yankner, 2013; Mattson and Camandola, 2001; Salminen et al., 2008; Zhang et al., 2013). NF-κB is a dimeric transcription factor consisting members of the Rel family, including Rel-A (p65), c-Rel, Rel-B, p50, and p52, and is often held in the cytoplasm by inhibitor IkB proteins as its latent form (Chen, 2005). Upon stimulation, the IκB kinase (IKK) complex phosphorylates the amino-terminal serine residues (S32 and S36) of IκBα, triggering its ubiquitination and degradation by the Skp-Cullin-F-box (SCF) Ub ligase complex and the 26S-proteasome pathway, respectively (Chen, 2005; Frescas and Pagano, 2008). Consequently, this allows the nuclear translocation of NF-κB p50-p65 complex for transcriptional activation of targeted genes. NF-κB activation in neurons occurs soon after brain ischemia as evidenced by IκBα degradation and p65 phosphorylation (Stephenson et al., 2000), which drives the neuronal expression of inflammatory mediators such as inter-leukin 6 (IL-6) (Ohtaki et al., 2006) and chemokine C-C motif ligand 2 (CCL2) (Stowe et al., 2012). Genetic and pharmacological studies targeting NF-κB-activating IKK have shown that inhibiting NF-κB is generally beneficial for stroke recovery (Herr-mann et al., 2005; Iadecola and Anrather, 2011). However, this has been challenged by stroke studies in mouse models with p50 or cRel deficiency (Harari and Liao, 2010), as well as in systemic injury models (Elsharkawy and Mann, 2007), suggesting that NF-κB-mediated acute inflammatory response is not just deleterious. In fact, the acute inflammation responses triggered by CNS injuries usually resolve within a short period of time, which set up tissue boundaries for subsequent repair process (Buckley et al., 2013; Iadecola and Anrather, 2011; Jin et al., 2010). However, brain-specific factors that govern inflammation resolution have not been well defined (Iadecola and Anrather, 2011). Hence, understanding the brain's regulatory mechanisms that ensure the timely activation and subsequent inactivation of NF-κB-mediated neuroinflammation is essential to develop a therapeutic strategy for the recovery and repair after ischemic brain injury.

Stroke mostly occurs in elderly people, and outcomes of stroke patients are highly influenced by age, indicating that aging is an inherent risk factor for stroke (Markus et al., 2005; Popa-Wagner et al., 2011). Compared to the young brain, the aged brain displays a

compromised ability to resolve stroke-mediated inflammation, causing high susceptibility to ischemia and poor functional recovery (Chen et al., 2010). Indeed, upon middle cerebral artery occlusion (MCAO), aged mice exhibit elevated proinflammatory mediators, large infarction volumes, severe behavioral impairment, and high mortality rates compared to young mice (DiNapoli et al., 2008; Jin et al., 2004; Liu et al., 2009; Rosen et al., 2005; Shapira et al., 2002), reflecting the effects seen in elderly patients who often experience severe functional disabilities following an ischemia (Hankey et al., 2002). However, little is known about brain-specific mechanisms that regulate the resolution of neuroinflammation that are potentially undermined during aging. Hence, investigating the timely regulation of NF-κB-mediated neuroinflammation is key to a better understanding of pathophysiology and repair after acute brain ischemia.

Here, we report that TRIM9 provides an innate mechanism to resolve ischemic-stroke-induced neuroinflammation via fine-tuning of *in vivo* NF-κB signaling activity in a mouse model, and thus, targeting TRIM9 and its related neuroinflammatory pathway may offer a target for immunomodulatory therapy for stroke.

RESULTS

TRIM9 Upregulation in the Peri-infarct Brain Region after Ischemic Stroke in Mice

Transient MCAO, which mimics ischemic stroke and reperfusion in rodents, is widely used to investigate post-ischemic inflammatory responses and resolution (Liesz et al., 2009; Shichita et al., 2009, 2012, 2017). Immunoblotting analysis of NF-κB activation showed that IκBα degradation and p65 phosphorylation were evidently induced between 1 and 12 hr after 30-min MCAO and returned close to a baseline level after 48 and 72 hr in C57BL/6J (wild-type [WT]) mice (Figures 1A and 1B). This was consistent with the self-limiting characteristics of post-ischemic inflammation (Liu et al., 2015) that preceded the repair processes (Iadecola and Anrather, 2011). We also observed the highly upregulated levels of p-p65 in NeuN-positive neurons of the ischemic brains at 12 hr after 30-min MCAO compared to those in the sham-operated group (Figures 1C and 1D). When ischemic brain tissues isolated 12 hr after surgical procedures were subjected to RNA sequencing (RNA-seq) analysis, the expression of numerous genes was altered in MCAO-treated tissues compared to those in sham-operated tissues (Figure 1E). Remarkably, among those top 20 upregulated genes, only *Trim9* exhibited a brain-specific expression pattern (Berti et al., 2002) (https://www.ncbi.nlm.nih.gov/gene/94090) (Figure S1A; Table S1). Gene ontology analysis showed that *Trim9* was in the neurological disease and inflammation pathway in which genes experienced the most significant alteration of expressions (adjusted p value < 0.01) (Figure 1F; Table S2). Immunoblotting assays showed the upregulation of TRIM9 in the ischemic brain hemisphere, when compared with the unaffected contralateral hemisphere (Figures S1B and S1C). In addition, high resolution *in situ* hybridization analysis with RNAscope gene-specific probes (Wang et al., 2012a) demonstrated that the upregulation of *Trim9* was primarily detected at the periphery of the ischemic areas in the ipsilateral hemisphere, as compared to a basal level of the unaffected contralateral hemisphere (Figure 1G). In addition, no significant difference of stroke-induced *Trim9* expression between 12-week-old male and female mice was observed (Figure S1D). Taken together, these findings

indicate that *Trim9* is highly upregulated in the peri-infarct cortical areas of mouse brain upon ischemic stroke.

Exacerbated Ischemic Brain Injury in *Trim9*-Deficiency Mice

Besides aberrant axonal branching in the corpus callosum (Winkle et al., 2014) and excessive dendritic arborization of den-tate granule cells in the hippocampus (Winkle et al., 2016b), *Trim9*-deficient (*Trim9*$^{-/-}$) mice exhibit no gross anatomical defects or impairment in motor functions (Winkle et al., 2016b). We found that the numbers of NeuN^{+} neurons, SMI-312^{+} neuritic density, Oligo2^{+} oligodendrocytes, NG2^{+}Oligo2^{+} oligodendrocyte precursor cells, GFAP^{+} astrocytes, and Iba1^{+} microglia in both the somatosensory cortex and hippocampus were nearly identical between *Trim9*$^{-/-}$ mice and WT *Trim9*$^{+/+}$ littermates (Figures S2A–S2F). In addition, consistent with the lack of expression in endothelial cells (Zhang et al., 2014), *Trim9*$^{-/-}$ mice showed no change of the middle cerebral artery (MCA) territory (Figures S2G and S2H) or alteration of cerebral blood flow (CBF) before, after, and during 30-min MCAO (Figures 2A and S2I) compared to WT littermates, indicating that the cerebrovascular system was not affected by *Trim9* deficiency. By contrast, *Trim9*$^{-/-}$ mice were more prone to ischemic injury than WT litter-mates, exhibiting a 2-fold increase in infarct volume (Figures 2B and 2C) and a 2.3-fold enhancement in edema volume (Figure 2C) at 24 hr after MCAO. Behavioral analysis using a 6-point motor neurological score method (Wang et al., 2005) showed an ~2-fold decline of neurological outcomes in *Trim9*$^{-/-}$ mice relative to WT littermates at 24 hr after MCAO (Figure 2C). Cytokines and chemokines are important mediators of neuroinflammation in stroke (Chamorro et al., 2012; Eltzschig and Carmeliet, 2011; Iadecola and Anrather, 2011). At 24 hr after 30-min MCAO, Trim9$^{-/-}$ mice showed a dramatic increase in a panel of inflammatory cytokines, including IL-6 and CCL2/5 but no alteration of IL-10 compared to WT littermates (Figures 2D and S3A). ELISA showed that tumor necrosis factor α (TNF-α) and IL-1β were marginally increased in Trim9$^{-/-}$ mice at 24 hr after 30-min MCAO but became more evident at 36 hr (Liesz et al., 2013) (Figure S3B). These data suggest TRIM9 functions in dampening neuronal expression of inflammation mediators of IL-6 and CCL2 that are upregulated within the first day of stroke (Ohtaki et al., 2006; Stowe et al., 2012). A terminal deoxynucleotidyl transferase dUTP nick-end labeling (TUNEL) assay and immunohistological analysis also indicated that the ischemic ipsilateral brain regions of *Trim9*$^{-/-}$ mice showed ~2-fold increases in apoptotic cells and neuronal death compared to those of WT lit termates (Figures 2E and 2F).

Trim9 Deficiency Causes the Elevation of Peripheral Immune Cell Infiltration in Mouse Brain

CCL2 (also known as monocyte chemoattractant protein-1) attracts inflammatory immune cells such as monocytes to infiltrate into brain parenchyma under pathological conditions, which triggers further neuronal dysfunction and damage (Mennicken et al., 1999). Flow cytometry analysis showed that compared to MCAO-treated WT littermates, MCAO-treated *Trim9*$^{-/-}$ mice had significant increases of CD45^{hi}GR1^{+}CD11b^{+} granulocytes and inflammatory monocytes and CD45^{hi}CD11b^{-}CD3e^{+} T cells (Figures 3). These results indicate that TRIM9 plays a critical role in dampening the stroke-induced production and recruitment of inflammation mediators and immune cells, respectively.

TRIM9 Suppresses Neuroinflammation by Inhibiting NF-κB Signaling

To further examine the role of TRIM9 in brain-specific NF-κB activation, ischemic brains were harvested 24 hr after MCAO and then subjected to immunoblotting analysis. This revealed increased IκBα degradation and p65 phosphorylation (p-p65) in the ischemic brains of *Trim9*$^{-/-}$ mice compared to those of *Trim9*$^{+/+}$ mice (Figures S4A and S4B). Consistently, immunostaining also showed increases of p-p65-positive neurons (NeuN) in the peri-infarct area of *Trim9*$^{-/-}$ mice (Figures S4C and S4D). To further test this, primary cortical neurons isolated from *Trim9*$^{+/+}$ and *Trim9*$^{-/-}$ embryos (Figure S5A) were challenged either by 30- or 60-min oxygen-glucose deprivation (OGD) with reoxygenation for 24 hr (R24h) or by the pro-inflammatory cytokine TNF-α or IL-1β for 30–120 min. Immunoblotting assays showed that the degradation of IκBα was more robust in *Trim9*$^{-/-}$ primary neurons upon stimulation with OGD (Figures 4A and 4B), TNF-α, or IL-1β (Figures S5B–S5E) than in *Trim9*$^{+/+}$ primary neurons. Correspondingly, the increase of p65 phosphorylation was also more evident in *Trim9*$^{-/-}$ primary neurons upon TNF-α or IL-1β stimulation than in *Trim9*$^{+/+}$ primary neurons (Figures S5B–S5E). Finally, human neural progenitor cell (hNPC)-derived neurons (Liang et al., 2016; Wang et al., 2016) were infected with scramble- or *TRIM9*-specific short hairpin RNA (shRNA) lentivirus for 24 hr, followed by OGD stimulation for 30- or 60-min shRNA-mediated knockdown of *TRIM9* expression in hNPC-derived neurons led to robust IκBα degradation and increased p65 phosphorylation upon OGD stimulation (Figures S5F and S5G). Furthermore, *TRIM9*-specific shRNA-treated hNPC-derived neurons were more vulnerable to OGD-induced cell death than scramble shRNA-treated neurons (Figures 4C and 4D). These results indicate that TRIM9 is required for neuronal survival under ischemia and inflammation.

As our previous study demonstrates the TRIM9-mediated suppression of NF-κB activation via its interaction with β-transducin repeat-containing protein (β-TrCP) (Shi et al., 2014), we further showed the TRIM9 and β-TrCP interaction in brain tissue of MCAO-treated or sham-operated mice (Figure 4E). In addition, primary neurons isolated from *Trim9*$^{-/-}$ embryos were infected with lentivirus containing vector, TRIM9-WT, or $S_{76}AS_{80}A$ (SA) mutant that no longer interacts with β-TrCP (Shi et al., 2014), followed by stimulation with OGD, TNF-α, or IL-1β. Our data showed that the substitution of TRIM9-WT allowed *Trim9*$^{-/-}$ primary neurons to regain their ability to suppress stimulation-induced NF-κB signaling, whereas the substitution of the TRIM9-SA mutant showed little or no effect on NF-κB signaling (Figures 4F, 4G, and S5H–S5K). When lentivirus-infected primary *Trim9*$^{-/-}$ neurons were treated with TNF-α and tested for the β-TrCP interaction with TRIM9 or IκBα, TRIM9-WT, but not TRIM9-SA mutant, effectively competed with IκBα for the β-TrCP interaction (Figure 4H). Consequently, *Trim9*$^{-/-}$ primary neurons showed a higher IκBα ubiquitination upon TNF-α + MG132 treatment than *Trim9*$^{+/+}$ primary neurons (Figure 4I). qRT-PCR also showed higher expression of the inflammatory mediators IL-6, TNF-α, IL-1β, and CCL2 in *Trim9*$^{-/-}$ primary neurons upon OGD stimulation than in *Trim9*$^{+/+}$ primary neurons (Figure 4J). These results indicate that TRIM9's interaction with β-TrCP is critical for fine-tuning NF-κB signaling and inflamma-tory responses in neurons.

AAV-PHP.B-Mediated Brain-wide TRIM9 Expression Ameliorates Ischemic Injury in Trim9$^{-/-}$ Mice

To explore whether *in vivo* brain-wide expression of *Trim9* could alleviate ischemia-induced neuroinflammation and brain injury in mice, we utilized an engineered variant of adeno-associated virus (AAV) serotype 9 (AAV-PHP.B) that can efficiently transfer genes throughout the CNS following systemic delivery (Deverman et al., 2016; Morabito et al., 2017). AAV-PHP.B-mediated expression of the green fluorescent protein (GFP), the Flag-tagged murine TRIM9-WT or the SA mutant was readily detected in *Trim9*$^{-/-}$ mouse embryonic fibroblasts (MEFs) and primary neurons (Figure S6A; see also STAR Methods). Subsequently, AAV-PHP.B:CAG-GFP (PHP.B-GFP), AAV-PHP.B:CAG-FLAG-TRIM9 (PHP.B-TRIM9), and AAV-PHP.B:CAG-FLAG-TRIM9-SA (PHP.B-SA) were administrated twice to 12-week-old *Trim9*$^{-/-}$ mice following a retro-orbital injection protocol (Deverman et al., 2016) (Figure 5A). GFP and FLAG-tagged TRIM9-WT or SA mutant expression were tested 21 days post-injection. Efficient expression of GFP, FLAG-tagged TRIM9-WT, or SA mutant was observed in neurons throughout the brain, including the cortex and hippocampus (Figures 5B and S6B). When compared with PHP.B-GFP- or PHP.B-SA-infected *Trim9*$^{-/-}$ mice 24 hr after 30-min MCAO, PHP.B-TRIM9-infected *Trim9*$^{-/-}$ mice showed substantially reduced infarct volume (Figures 5C and 5D) and neurological impairments, as indicated by neurological scores (Figure 5E). An immunoblotting assay of tissue extracts from MCAO-induced ischemic brain hemispheres showed the reduced IκBα degradation in PHP.B-TRIM9-infected *Trim9*$^{-/-}$ mice compared to PHP.B-GFP- or PHP.B-SA-infected *Trim9*$^{-/-}$ mice (Figures S6C and S6D). Finally, when primary neurons isolated from *Trim9*$^{-/-}$ mice were infected with PHP.B-GFP, PHP.B-TRIM9, or PHP.B-SA and then subjected to OGD conditions, IκBα degradation was considerably lower in PHP.B-TRIM9-infected *Trim9*$^{-/-}$ neurons than in PHP.B-GFP- or PHP.B-SA-infected *Trim9*$^{-/-}$ neurons (Figures S6E and S6F). These results collectively indicate that AAV-PHP.B-mediated brain-wide TRIM9 expression effectively resolves inflammatory responses in neurons, providing neuroprotection against ischemic stroke.

AAV-PHP.B-Mediated Brain-wide TRIM9 Expression Alleviates Ischemic Injury in Middle-Aged Mice

A previous genome-wide analysis reports that the stroke-induced expression of a specific group of genes, including *Trim9*, is considerably lower in the ipsilateral cortex of aged rats than in that of young rats (Buga et al., 2012). A similar level of TRIM9 expression in the brain was observed between 12-week-old young mice and 70-week-old middle-aged mice under normal conditions. In contrast, the stroke-induced upregulation of TRIM9 expression was detectably lower in aged mouse brains than in young mouse brains (Figures 6A and 6B). The stroke-induced expression of two key inflammatory mediators, IL-6 (Figures 6C and 6D) and CCL2 (Figures 6E and 6F), was induced much higher in aged mouse brains than in young mouse brains.

To examine *in vivo* expression of *Trim9* to alleviate ischemia-induced neuroinflammation in aged mice, 70-week-old C57BL/6J mice were retro-orbitally injected with PHP.B-GFP or PHP.B-TRIM9 and subjected to 30-min MCAO, followed by neurological tests at 24 hr. When compared with PHP.B-GFP-infected aged mice, PHP.B-TRIM9-infected aged mice

showed substantially reduced infarct areas (Figures 6G and 6H) and neurological impairments, as indicated by neurological scores (Figure 6I). Confocal microscopy showed that compared to PHP.B-GFP-infected aged mice, PHP.B-TRIM9-infected aged mice had reduced levels of p-p65-positive neurons (NeuN) in the peri-infarct cortex (Figures 6J and 6K) and neuronal cell death, as indicated by $TUNEL^{+}NeuN^{+}$ double-positive cells in the infarct cortex (Figures 6L and 6M). The strong correlation between the p-p65-positive neuron population level and the motor neurological behavior score was observed in PHP.B-GFP- or PHP.B-TRIM9-infected aged mice (Figure 6N). These results collectively demonstrate that AAV-PHP.B-mediated brain-wide TRIM9 expression effectively alleviates neuroinflammation and ameliorates neuropathological and neurological outcomes after ischemic stroke.

DISCUSSION

The acute inflammatory response and its resolution are indispensable for body's physiological repair process after injuries, while unresolved inflammation is implicated in a body of human diseases, including CNS injuries (Schwartz and Baruch, 2014). Inflammation resolution in the CNS is a highly organized active process that requires complex crosstalk between injured neurons, glial cells, and infiltrating inflammatory cells (Schwartz and Baruch, 2014). However, brain factors that govern the resolution of neuroinflammation are yet to be defined (Iadecola and Anrather, 2011). By revisiting the brain's endogenous genes within the inflammatory response network that were activated upon ischemic injury, we identified TRIM9 as a brain-specific modulator of NF-κB-dependent neuroinflammation (Figure 1). It governs the resolution of post-ischemic inflammation and consequently improves neuropathological and neurological outcomes in the mouse model of acute ischemic stroke (Figure 2). Accordingly, *Trim9* deficiency is accompanied by elevated pro-inflammatory cytokine production, inflammatory cell infiltration, subsequent neuronal death, and exacerbated brain injury after MCAO (Figures 2 and 3).

Pro-inflammation, anti-inflammation, and pro-resolution signals converge on the NF-κB pathway. In acute ischemia, NF-κB activation in injured neurons initiates strong inflammatory responses via production of proinflammatory mediators. TRIM9 expression is strongly increased in the peri-infarct area in a mouse stroke model (Figure 1G). This delayed surge of *Trim9* expression ensures timely antagonization of NF-κB activity and tissue resolution of inflammation, as we showed that the brain-wide expression of TRIM9 effectively promoted resolution of neuroinflammation and alleviated neuronal death in TRIM9-deficient mice (Figure 5). Our findings indicated that the balance between these pathways could be adjusted temporally by TRIM9 after ischemic stroke. AAV-PHP.B-mediated TRIM9 expression ameliorates the ischemic neuropathology and neurological outcomes in young $Trim9^{-/-}$ mice (Figure 5) and 70-week-old WT mice (Figure 6). This suggests that targeting TRIM9 for better resolution of neuroinflammation may offer a potential target for immunomodulatory therapy for acute ischemia. Previous studies have shown that the infiltration pattern of peripheral immune cells and timing of immune activation differ in stroke (Chamorro et al., 2012; Iadecola and Anrather, 2011; Jin et al., 2010), suggesting that the infarct or behavior could possibly change over time. Investigation

of stroke-related neuropathology on later time-point than 24 hr could provide more useful information about the resolution of inflammation, especially in aged mice.

Older women have a much higher incidence of stroke than men as well as a worse prognosis, which is recapitulated in rodent model; for instance, aged female mice display a larger infarct volume upon stroke than aged male mice (Liu et al., 2009). In the current study, aged female mice were specifically chosen to evaluate the therapeutic potential of AAV-based gene therapy, since TRIM9 expression was similar between young male and female mice (Figure S1D). As a huge body of literature on stroke and inflammation has used young male mice as MACO animal models (Herrmann et al., 2005; Kawano et al., 2006; Liesz et al., 2009, 2013; Reischl et al., 2014; Sarabi et al., 2008; Shichita et al., 2009, 2012, 2017; Strecker et al., 2011; Wang et al., 2016), and we also utilized young male mice to maintain consistency with previous studies. It is well known that the aged population is not only highly susceptible to ischemic stroke but also shows slow recovery from ischemic stroke. However, the basis of this high susceptibility and slow recovery of the aged population is very complex, with numerous contributing factors. We found that the upregulation of TRIM9 expression appeared to be critical to resolve inflammation in the peri-infarct region of brain and minimize the injury size. However, this stroke-induced upregulation of TRIM9 expression was compromised in aged mice, causing sustained neuroinflammation and enhanced ischemic damage. Induction of *Trim9* expression in the peri-infarct areas of ischemic brain occurred during the early stage. Additional studies are necessary to understand the molecular mechanism of Trim9 expression under normal conditions versus ischemic stroke conditions.

The MCAO model we used here is an acute stroke mouse model, which does not allow a sufficient time window for target gene delivery for gene therapy. For example, while AAV mutant AAV-PHP.B enabled brain-wide expression of TRIM9 gene with high efficiency (Deverman et al., 2016), TRIM9 gene delivery still required days (or even more than a week) after AAV injection. Alternative methods to quickly upregulate endogenous TRIM9 expression may provide its systemic expression for post-stroke treatment. Lastly, the pre-stroke strategies may be utilized as prevention approaches, which would represent a potential therapeutic method for the aging population, especially in at-risk older women. Further study is needed to evaluate a number of methods to upregulate brain-specific TRIM9 expression.

Parkinson’s disease (PD), the second most common age-associated neurodegenerative disorder, is characterized by the loss of dopaminergic neurons (Obeso et al., 2010), as well as chronic neuroinflammation (McGeer and McGeer, 2004). Specifically, post-mortem analyses of human PD patients and experimental animal studies shows that the chronic increase of proinflammatory cytokines and the infiltration and accumulation of immune cells from the periphery are also implicated in the pathogenesis of PD (Barcia et al., 2003; Hirsch and Hunot, 2009; Hirsch et al., 2012). Intriguingly, a previous study showed that Trim9 expression was significantly downregulated in the brains of PD and Lewy body dementia (Tanji et al., 2010). We showed that AAV-PHP.B-mediated Trim9 expression markedly reduced neuroinflammation in young Trim9$^{-/-}$ mice (Figure 5) and middle-aged WT mice (Figure 6), leading to improvement of the ischemic neuropathology and neurological

outcomes. This suggests that manipulating Trim9 expression for better resolution of neuroinflammation may offer prospect to immunomodulatory therapy for PD, ischemic stroke, and even other neurodegenerative diseases. A better understanding of the role of TRIM9-mediated regulation of inflammation would provide insight into the neuropathological processes and help to establish effective therapeutic strategies.

STAR★METHODS

CONTACT FOR REAGENT AND RESOURCE SHARING

Further information and request for resources and reagents should be directed to and will be fulfilled by Lead Contact Jae U. Jung (jaeujung@med.usc.edu).

EXPERIMENTAL MODEL AND SUBJECT DETAILS

Cell culture—HEK293 cells were purchased from ATCC (catalog # CRL-11268; the sex is female) and maintained in DMEM supplemented with 10% fetal bovine serum (FBS) and 100 U ml^{-1} penicillin-streptomycin. IL-1β (Biolegend, catalog # 575102), TNF-α (Biolegend, catalog # 575202), and proteasome inhibitor MG132 (R&D Systems, catalog # 1748) were used for stimulation on mouse primary neurons.

Mouse primary neuron culture—Cerebral cortices from E18 mouse embryos (the sex is unavailable) were dissected, carefully stripped of their meninges, digested with TrypLE Express Enzyme (Thermo Fisher Scientific, catalog # 12604013) with DNaseI (0.5 mg/ml) (Sigma, catalog # AMPD1) for 20 min at 37°C, and dispersed to single-cell level by passing through a cell strainer (70 μm). The cell suspension was then cultured with Neurobasal medium supplemented with B27 Supplement (Thermo Fisher Scientific, catalog # 17504044) at 37°C in humiliated 5% CO_2, 95% air on poly-D-Lysine (Millipore, catalog # A-003-E) and laminin (Thermo Fisher Scientific, catalog # 23017015) pre-coated coverslips or in 12-well culture plates. Medium was replaced at 50% every other day.

Human neural progenitor cell (hNPC)-derived neurons—Human neural progenitor cell (hNPC) from fetal origin (the sex is unavailable) (Guo et al., 2013; Wang et al., 2010) were maintained as neurospheres in DMEM/F12-N2 supplemented with 20 ng/ml (1.4 nM) bFGF (Sigma-Aldrich, St. Louis, MO) in low-attachment T-25 flasks (Corning, Acton, MA) (Wang et al., 2016). For differentiation, hNPC were plated on poly-L-Orthithine (10 μg/ml) and laminin (10 μg/ml) coated round cover glasses in 4-well plates at a density of 4×10^5 per well in STEMdiff Neuron Maturation medium (StemCell Technologies, Inc.) and incubated for 10 days *in vitro* to allow for differentiation.

Mouse embryo fibroblasts (MEFs)—MEFs from *Trim9*$^{-/-}$ mice (the sex is unavailable) was isolated and cultured, as previously described (Durkin et al., 2013). Briefly, E13 embryos were harvested and digested by 0.25% trypin-EDTA. Cell suspension was cultured with MEF culture medium containing DMEM supplemented with 10% FBS and 100 U ml^{-1} penicillin-streptomycin in T75 flasks.

Mice—The Institutional Animal Care and Use Committee at the University of Southern California approved all procedures per the National Institutes of Health guidelines. Mice were housed in plastic cages on a 12h light cycle, with *ad libitum* access to water, with standard laboratory diet, and in a specific pathogen-free facility. *Trim9*$^{+/-}$ heterozygous mice (Winkle et al., 2014) were bred to generate age-matched *Trim9*$^{-/-}$ and littermates *Trim9*$^{+/+}$ mice. Male (Liesz et al., 2009; O'Collins et al., 2006; Shichita et al., 2009, 2012) *Trim9*$^{+/+}$ and *Trim9*$^{-/-}$ mice with 12-week-old were used. C57BL/6J mice were purchased from the Jackson Laboratory (JAX stock 000664). Because there is a significant *sex* effect on the pathology of brain ischemia (Liu et al., 2009; Wendeln et al., 2018), where both male and female mice were compared, only female aged C57BL/6J mice with 70-week-old were used in the present study. All the animals that survived surgical procedures were included in the study. All animals were randomized for all stroke studies and procedures. All experiments were blinded; the operators responsible for experimental procedure and data analysis were blinded and unaware of group allocation throughout the experiments.

METHOD DETAILS

Transient middle cerebral artery occlusion (MCAO)—Using a 27-½ gauge needle, mice were anesthetized with 100 mg/kg Ketamine intraperitoneally (IP) and 10 mg/kg IP xylazine. Rectal temperature was maintained at 37°C using a feedback-controlled heating system. MCA was occluded for 30 minutes using a silicon-coated nylon monofilament (DOCCOL, CO) as we previously described (Wang et al., 2012b). Cerebral blood flow was monitored by laser Doppler flowmetry (Transonic Systems). Mice with an adequacy of MCAO as evidenced by R 80% drop in the cerebral blood flow were included in the study. Motor neurological examination was determined after 24 hours, using the following criteria: no neurological deficit, 0; failure to extend left forepaw fully, 1; turning to left, 2; circling to left, 3; unable to walk spontaneously, 4; and stroke-related death, 5. All mice were euthanized 0, 1, 4, 12, 24, 36, 48, or 72 hours after the MCAO for indicated analysis. All animals that were survived from surgical procedures were included in the study.

Immunoblotting—Brain tissue or cell lysates were collected in 1% NP40 buffer with the protease inhibitor cocktail (Roche, catalog # 4693159001) and phosphatase inhibitor PhosSTOP (Roche, catalog # 4906845001), and protein amounts were quantified by BCA protein assay kit (Thermo Fisher Scientific, catalog # 23227). Proteins were separated by SDS-PAGE and transferred to PVDF membrane (Bio-Rad, catalog # 1620177)) by semi-dry transfer at 25V for 30 min. All membranes were blocked in 5% milk in PBST for 1 h and probed overnight with indicated primary antibodies in 5% BSA at 4°C. Primary antibodies included: mouse monoclonal anti-IκBα antibody (Cell Signaling, catalog # 9247, 1:2000), rabbit monoclonal anti-phospho-IκBα antibody (Cell Signaling, catalog # 2859, 1:1000), rabbit monoclonal anti-phospho-p65 antibody (Cell Signaling, catalog # 3033, 1:1000), mouse monoclonal anti-β-actin antibody (Santa Cruz, catalog # sc-47778, 1:2000), rabbit polyclonal anti-TRIM9 antibody (Winkle et al., 2014) (1:2000, generated using murine TRIM9 recombinant protein aa 158–271; reacting with three isoform a/b/c), mouse monoclonal anti-ubiquitin antibody (Santa Cruz, catalog # sc-8017, 1:1000), rabbit monoclonal anti-β-TrCP antibody (Cell Signaling, catalog # 4394, 1:1000), mouse monoclonal anti-HA antibody (Santa Cruz, catalog # sc-57594, 1:2000), mouse monoclonal

anti-GFP antibody (Santa Cruz, catalog # sc-101525, 1:2000), and mouse monoclonal anti-Flag antibody (Sigma, catalog # F1804, 1:2000). Appropriate HRP-conjugated secondary antibodies were incubated on membranes in 5% milk and bands were developed with ChemiDoc Touch imaging system (Bio-Rad) and analyzed in Image Lab software.

Tissue staining—At endpoint, mice were anesthetized and transcardially perfused with PBS and fixed with 4% PFA. Mouse brains were post-fixed overnight in 4% PFA at 4°C. For cryosectioning, fixed tissues were cryoprotected in 30% sucrose in PBS overnight at 4°C and embedded in Tissue-Tek OCT compound (VWR, catalog # 25608–930). Cryostat sections were cut at 20 μm thickness. Mouse brain sections were permeabilized in PBS-T (PBS containing 0.2% Triton X-100) for 10 min, blocked with 5% normal donkey serum (Jackson ImmunoResearch, catalog # 017-000-121) for 60 min and incubated in primary antibody diluted in the blocking solution overnight at 4°C. Primary antibodies used in this study include mouse monoclonal anti–glial fibrillary acidic protein (GFAP) (cell signaling, catalog # 3670), Rabbit monoclonal anti-Iba1 (Abcam, catalog # ab178846), Rabbit polyclonal anti-NeuN (Millipore, catalog # ABN78), Mouse monoclonal anti-NeuN (Millipore, catalog # MAB377), Mouse monoclonal anti-SMI-312 (Abcam, catalog # ab24574), Rabbit polyclonal anti-NG2 (Abcam, catalog # ab83178), Mouse monoclonal anti-Olig2 (Abcam, catalog # MABN50), Mouse monoclonal anti-Flag (Sigma, catalog # F1804), Rabbit monoclonal anti-phospho-p65 (Cell Signaling, catalog # 3033), Rat monoclonal anti-IL6 (Thermo Fisher Scientific, catalog # AMC0864), and Rabbit polyclonal anti-CCL2 (Abcam, catalog # 9779). After three washes with PBS, sections were incubated with the secondary antibodies for 1 h, including Alexa 488-conjugated donkey anti-mouse (Thermo Fisher Scientific, catalog # A21202), Alexa 488-conjugated donkey anti-rabbit (Thermo Fisher Scientific, catalog # A-21206), Alexa 568-conjugated donkey anti-mouse (Thermo Fisher Scientific, catalog # A10037), Alexa 568-conjugated donkey anti-rabbit (Thermo Fisher Scientific, catalog # A10042), Alexa 647-conjugated donkey anti-rabbit (Thermo Fisher Scientific, catalog # A-31573), Alexa 488-conjugated donkey anti-rat (Thermo Fisher Scientific, catalog # A-21208), and Alexa 647-conjugated donkey anti-rat (Jackson ImmunoResearch Laboratories, catalog # 712-605-153). All images were taken with the Zeiss 510 confocal microscopy or using the BZ 9000 all-in-one Fluorescence Microscope from Keyence (Osaka, Japan), and analyzed using NIH ImageJ software.

RNA sequencing—RNA was prepared using TRIzol Reagent (Thermo Fisher Scientific, catalog # 15596018) followed by RNeasy Mini Kit (QIAGEN, catalog # 74104). The libraries were made using KAPA stranded mRNA-seq kits (KAPA Biosystems, catalog # kk8421) according to manufacturer's protocol. The cDNA libraries were sent to the Technology Center for Genomics & Bioinformatics at UCLA for sequencing on HiSeq 3000 with single end read (~30 million reads per sample). RNA-seq data was inspected by FastQC (Simon, 2010). Using default settings, STAR version 2.5.2b (Dobin et al., 2013) were used to map reads to mouse genome GRCm38. Alignment results were processed for gene quantification using featureCounts version 1.5.1 (Liao et al., 2014) with the second strand-specific option. Differentially expressed genes were determined using DESeq2 version 1.14.1 (Love et al., 2014). The significantly changed genes were analyzed using the Ingenuity Pathway Analysis tool for functional analysis. The comparison of expression

levels of the upregulated genes was performed by RPKM value of each gene from existing RNaseq data in NCBI.

RNAscope *in situ* hybridization—*Trim9* mRNA transcripts were detected using murine gene-specific probe (Advanced Cell Diagnotics, catalog # 479071) and visualized using the RNAscope 2.5 HD Reagent Kit RED (Advanced Cell Diagnotics, catalog # 322360) on 4% paraformaldehyde (PFA) fixed frozen mouse brain tissue sections, according the manufacturer's instructions, followed by counterstaining with hematoxylin (Vector Laboratories, catalog # H3401). Sections were imaged using the BZ 9000 all-in-one Fluorescence Microscope from Keyence (Osaka, Japan), and analyzed using NIH ImageJ software.

Visualization of the anastomotic line between the middle cerebral artery (MCA) and anterior cerebral artery (ACA)—We performed an assay with the procedures as previously described (Wang et al., 2005). Briefly, latex mixed with carbon black was injected through the cannulated aorta of mouse. Anastomotic lines between the MCA and the ACA territories were determined by tracing peripheral branches on dorsal brain surfaces of mice to the points at which vessels were connected (dotted red line).

Cresyl violet staining and neuropathological analysis—Mouse brain sections from five equidistant rostrocaudal brain levels, at −1.6 mm, 0.8 mm, 0 mm, 0.8 mm and 1.6 mm from bregma, were fixed by methanol and stained with the Cresyl Echt Violet staining − kit (American − MasterTech, catalog # AHC0443). Sections were digitized and transformed into gray model, and the border between infarct and non-infarct tissue was outlined using an image analysis system (ImageJ). On these sections, infarct volume and brain swelling were quantified. The infarct volume was calculated by subtracting the volume of the non-lesioned area in the ipsilateral hemisphere from the volume of the whole area in the contralateral hemisphere (Wang et al., 2013). The edema volume was calculated by subtracting the volume of the contralateral hemisphere from the volume of the ipsilateral hemisphere (Wang et al., 2005).

RT-qPCR—Total RNAs were extracted from mouse brain tissues or mouse primary neurons using TRIzol Reagent (Thermo Fisher Scientific, catalog # 15596018) followed by RNeasy Mini Kit (QIAGEN, catalog # 74104) according to the manufacturer's instructions. The purified RNA was reversely transcripted to cDNA using iScript cDNA Synthesis Kit (Bio-Rad, catalog # 1708891). All gene transcripts were quantified by quantitative PCR using iQ SYBR Green supermix (Bio-Rad, catalog # 1708880) on CFX96 real-time PCR system (Bio-Rad). Primer sequences are listed in Table S3.

ELISA—Mouse brain tissues were isolated and homogenized mechanically. The resulting supernatants were collected and their concentration of IL-6, IL-1β, TNF-α or IL-10 was determined with a mouse-specific ELISA kit (BD Biosciences, catalog # 555240 for IL-6, 559603 for IL-1β, 555268 for TNF-α, 555252 for IL-10), and this was followed by analysis with the FilterMax F5 multi-mode microplate reader (Molecular Devices).

TUNEL staining—Terminal deoxynucleotidyl transferase-mediated dUTP nick endlabeling (TUNEL) assay was employed to demonstrate apoptotic cells. Using the *In Situ* Cell Death Detection Kit, Fluorescein (Roche, catalog # 11684795910) or *In Situ* Cell Death Detection Kit, TMR red (Roche, catalog # 12156792910), brain sections were treated following the procedure specified by the manufacturer.

Analyzing infiltrating immune cells—The mice were transcardially perfused with PBS containing 0.05 M EDTA extensively to remove blood cells in the circulation. The forebrain (bregma from −3 to 3) of the hemisphere was removed and dissociated using neural tissue dissociation kit (MACS Miltenyl Biotec, catalog # 130093231). Ipsilateral (ischemic) hemisphere of the forebrain was used while contralateral hemisphere of the fore-brain was used as sham control. Debris was removed by Debris Removal Solution (MACS Miltenyl Biotec, catalog # 130109398) followed by removal of red blood cells (Biolegend, catalog # 420301). Cell suspensions were stained with propidium iodide (Invitrogen, catalog # P3566) and fluorochrome-conjugated antibodies including CD45 (APC/Cy7, 1:100, catalog # 103116), CD11b (eFluor450, 1:100, catalog # 48-0112-82), CD11c (PE/Cy7, 1:100, catalog # 117318), CD3e (PerCP/Cy5.5, 1:100, catalog # 100328), or GR1 (APC, 1:100, catalog # 108412). Subsequently, the stained suspensions were analyzed with BD FACSCanto II flow cytometer and analyzed with FlowJo software. Each cell type was indicated by percentage of CD45 positive cells. All antibodies were purchased from eBioscience or BD PharMingen. Propidium iodide staining was used to gate live cells.

Immunocytochemistry—Cultured mouse primary neurons were fixed with 4% PFA at room temperature for 20 min, permeabilized, and stained with primary antibodies, including rabbit polyclonal anti-TRIM9(Winkle et al., 2014) and mouse monoclonal anti-MAP2 (Abcam, catalog # ab11267), followed by incubation of secondary antibodies including Alexa 488-conjugated donkey anti-mouse (Thermo Fisher Scientific, catalog # A21202) and Alexa 568-conjugated donkey anti-rabbit (Thermo Fisher Scientific, catalog # A10042). All images were taken with the BZ 9000 all-in-one Fluorescence Microscope from Keyence (Osaka, Japan) and analyzed using NIH ImageJ software.

Oxygen and Glucose Deprivation (OGD)—Mouse primary cortical neurons or hNPC-derived neurons were treated with OGD by replacing culture medium with a glucose-free Neurobasal medium (Thermo Fisher Scientific, catalog # 21103049), and they were immediately placed in a hypoxic incubator chamber (STEMCELL, catalog # 27310) flushed with a gas mixture of 94%N_2/5%CO_2/1%O_2. After OGD for the indicated time, medium was replaced by standard medium, and cells were cultured under normal condition for reoxygenation of 24 h.

Lentivirus infection—Lentiviral vector-mediated *in vitro* gene delivery was performed as previously described (Shi et al., 2014). Briefly, hNPC-derived neurons or mouse primary neurons were cultured with medium containing 5 μg/ml polybrene (Sigma, catalog # H9268) and 5×10^5 infectious units of lentiviruses containing the following: scrambled shRNA, *TRIM9*-specific shRNAs (target sequence for human: 5-CGATGCCCTCAACAGAAGAAA-3), pCDH lentivirus expressing mouse HA-TRIM9, or

pCDH lentivirus expressing HA-SA mutant of TRIM9. At 48 h post infection, cells were further treated with OGD or other conditions as indicated.

Live-Dead Cell assay—hNPC-derived neurons were washed with PBS. LIVE-DEAD Viability/Cytotoxicity Kit (Thermo Fisher Scientific, catalog # L3224) was used to quickly discriminate live from dead cells by simultaneously staining with green-fluorescent calcein-AM to indicate intracellular esterase activity and red-fluorescent ethidium homodimer-1 to indicate loss of plasma membrane integrity. The samples were immediately imaged by the BZ 9000 all-in-one Fluorescence Microscope from Keyence (Osaka, Japan) and analyzed using ImageJ software.

Immunoprecipitation—For co-IPs, brain tissues and cells were lysed with RIPA minimum lysis buffer (Millipore, catalog # 20–188)). After clarification and pre-clearing, protein amounts were quantified by BCA protein assay kit (Thermo Fisher Scientific, catalog # 23227). 1/10 of cell lysates were heated as whole cell lysate in immunoblotting, and the remained 9/10 lysates were incubated for 16 h with indicated antibodies, followed by additional incubation with Pierce Protein A/G Agarose (Thermo Fisher Scientific, catalog # 20422) for 2h. Immune complexes were washed with lysis buffer and subjected to immunoblotting analysis. For ubiquitination, cells were initially lysed with RIPA buffer containing 1% SDS, then cell extracts were diluted with RIPA buffer to 0.1% SDS concentration. Finally 1/9 of the diluted extracts were heated as whole cell lysate in immunoblotting and the remained 9/10 lysates were subjected to IP and IB.

Adenovirus associated virus (AAV) mediated *in vivo* delivery of Trim9—For *in vivo* delivery of *Tirm9* to the central nervous system, we intravenously injected 12-week-old *Trim9*$^{-/-}$ mice or 70-week-old C57BL/6J mice at *retro-orbital* site using a AAV-PHP.B vector, a method that allows widespread gene transfer to the adult brain (Deverman et al., 2016), either expressing mouse *Trim9* (NM_001110203.1) under the control of a CAG promoter (AAVPHP.B:CAG-TRIM9), TRIM9-SA mutant (AAV-PHP.B:CAG-TRIM9-SA), or a control vector encoding the green fluorescent protein (AAV-PHP.B:CAG-GFP). Retro-orbital injections of 1.5×10^{12} genome copies per mouse was performed twice at 21 and 18 days before MCAO, to allow sufficient re-expression of TRIM9 in the CNS.

QUANTIFICATION AND STATISTICAL ANALYSIS

The sample size chosen for our animal experiments in this study was estimated based on our prior experience performing similar experiments. For all the bar graphs, data was expressed as mean ± s.d. The various types of statistical analysis were performed using GraphPad Prism and by an investigator blinded to the experimental conditions, including two-way ANOVA test, Mann-Whitney *U* test, Wilcoxon matched pair test, one-way ANOVA followed by Tukey's post hoc analysis, one-way ANOVA followed by Bonferroni's post hoc analysis, and two-tailed Student's t test was performed using GraphPad Prism. $P\ value < 0.05$ was considered statistically significant.

DATA AVAILABILITY

The RNA-seq data has been deposited to the NCBI GEO database under the accession number GEO: GSE114652.

Supplementary Material

Refer to Web version on PubMed Central for supplementary material.

ACKNOWLEDGMENTS

This research was supported in part by the NIH (grants CA200422, CA180779, DE023926, DE027888, DE28521, AI073099, AI116585, AI129496, AI140718, and AI140705), the Hastings Foundation, and the Fletcher Jones Foundation (J.U.J.); NIH grant 9R01NS090904-16 (B.V.Z.); the Alzheimer's Association (grant NIRG-15-363387) and Whittier Foundation (Z.Z.); the Cure for Alzheimer's Fund (B.V.Z. and Z.Z.), NS090904, and Foundation Leducq Translatlantic Network of Excellence for the Study of Perivascular Spaces in Small Vessel Disease (reference 16 CVD 05) (B.V.Z.); and GM108970 (S.L.G.). We acknowledge funding from the Beckman Institute at Caltech (to V.G. and B.E.D.) through the Resource Center for CLARITY, Optogenetics, and Vector Engineering. V.G. is a Heritage Principal Investigator supported in this work by an NIH Director's New Innovator Award (DP20D017782 to V.G.).

REFERENCES

Barcia C, Fernández Barreiro A, Poza M, and Herrero MT (2003). Parkinson's disease and inflammatory changes. Neurotox. Res 5, 411–418. [PubMed: 14715444]

Benjamin EJ, Blaha MJ, Chiuve SE, Cushman M, Das SR, Deo R, de Ferranti SD, Floyd J, Fornage M, Gillespie C, et al.; American Heart Association Statistics Committee and Stroke Statistics Subcommittee (2017). Heart Disease and Stroke Statistics-2017 Update: a report from the American Heart Association. Circulation 135, e146–e603. [PubMed: 28122885]

Berti C, Messali S, Ballabio A, Reymond A, and Meroni G (2002). TRIM9 is specifically expressed in the embryonic and adult nervous system. Mech. Dev 113, 159–162. [PubMed: 11960705]

Buckley CD, Gilroy DW, Serhan CN, Stockinger B, and Tak PP (2013). The resolution of inflammation. Nat. Rev. Immunol 13, 59–66. [PubMed: 23197111]

Buga AM, Scholz CJ, Kumar S, Herndon JG, Alexandru D, Cojocaru GR, Dandekar T, and Popa-Wagner A (2012). Identification of new therapeutic targets by genome-wide analysis of gene expression in the ipsilateral cortex of aged rats after stroke. PLoS ONE 7, e50985. [PubMed: 23251410]

Chamorro Á, Meisel A, Planas AM, Urra X, van de Beek D, and Veltkamp R (2012). The immunology of acute stroke. Nat. Rev. Neurol 8, 401–410. [PubMed: 22664787]

Chamorro Á, Dirnagl U, Urra X, and Planas AM (2016). Neuroprotection in acute stroke: targeting excitotoxicity, oxidative and nitrosative stress, and inflammation. Lancet Neurol. 15, 869–881. [PubMed: 27180033]

Chen ZJ (2005). Ubiquitin signalling in the NF-kappaB pathway. Nat. Cell Biol 7, 758–765. [PubMed: 16056267]

Chen RL, Balami JS, Esiri MM, Chen LK, and Buchan AM (2010). Ischemic stroke in the elderly: an overview of evidence. Nat. Rev. Neurol 6, 256–265. [PubMed: 20368741]

Deverman BE, Pravdo PL, Simpson BP, Kumar SR, Chan KY, Banerjee A, Wu WL, Yang B, Huber N, Pasca SP, and Gradinaru V (2016). Cre-dependent selection yields AAV variants for widespread gene transfer to the adult brain. Nat. Biotechnol 34, 204–209. [PubMed: 26829320]

DiNapoli VA, Huber JD, Houser K, Li X, and Rosen CL (2008). Early disruptions of the blood-brain barrier may contribute to exacerbated neuronal damage and prolonged functional recovery following stroke in aged rats. Neurobiol. Aging 29, 753–764. [PubMed: 17241702]

Dobin A, Davis CA, Schlesinger F, Drenkow J, Zaleski C, Jha S, Batut P, Chaisson M, and Gingeras TR (2013). STAR: ultrafast universal RNA-seq aligner. Bioinformatics 29, 15–21. [PubMed: 23104886]

Durkin ME, Qian X, Popescu NC, and Lowy DR (2013). Isolation of mouse embryo fibroblasts. Bio. Protoc 3, e908.

Elsharkawy AM, and Mann DA (2007). Nuclear factor-kappaB and the hepatic inflammation-fibrosis-cancer axis. Hepatology 46, 590–597. [PubMed: 17661407]

Eltzschig HK, and Carmeliet P (2011). Hypoxia and inflammation. N. Engl. J. Med 364, 656–665. [PubMed: 21323543]

Frescas D, and Pagano M (2008). Deregulated proteolysis by the F-box proteins SKP2 and beta-TrCP: tipping the scales of cancer. Nat. Rev. Cancer 8, 438–449. [PubMed: 18500245]

Gabuzda D, and Yankner BA (2013). Physiology: inflammation links ageing to the brain. Nature 497, 197–198. [PubMed: 23636321]

Guo H, Zhao Z, Yang Q, Wang M, Bell RD, Wang S, Chow N, Davis TP, Griffin JH, Goldman SA, and Zlokovic BV (2013). An activated protein C analog stimulates neuronal production by human neural progenitor cells via a PAR1-PAR3-S1PR1-Akt pathway. J. Neurosci 33, 6181–6190. [PubMed: 23554499]

Hankey GJ, Jamrozik K, Broadhurst RJ, Forbes S, and Anderson CS (2002). Long-term disability after first-ever stroke and related prognostic factors in the Perth Community Stroke Study, 1989–1990. Stroke 33, 1034–1040. [PubMed: 11935057]

Hao JC, Adler CE, Mebane L, Gertler FB, Bargmann CI, and Tessier-Lavigne M (2010). The tripartite motif protein MADD-2 functions with the receptor UNC-40 (DCC) in Netrin-mediated axon attraction and branching. Dev. Cell 18, 950–960. [PubMed: 20627077]

Harari OA, and Liao JK (2010). NF-κB and innate immunity in ischemic stroke. Ann. N Y Acad. Sci 1207, 32–40. [PubMed: 20955423]

Herrmann O, Baumann B, de Lorenzi R, Muhammad S, Zhang W, Kleesiek J, Malfertheiner M, Köhrmann M, Potrovita I, Maegele I, et al. (2005). IKK mediates ischemia-induced neuronal death. Nat. Med 11, 1322–1329. [PubMed: 16286924]

Hirsch EC, and Hunot S (2009). Neuroinflammation in Parkinson's disease: a target for neuroprotection? Lancet Neurol. 8, 382–397. [PubMed: 19296921]

Hirsch EC, Vyas S, and Hunot S (2012). Neuroinflammation in Parkinson's disease. Parkinsonism Relat. Disord 18 (Suppl 1), S210–S212. [PubMed: 22166438]

Iadecola C, and Anrather J (2011). The immunology of stroke: from mechanisms to translation. Nat. Med 17, 796–808. [PubMed: 21738161]

Jin K, Minami M, Xie L, Sun Y, Mao XO, Wang Y, Simon RP, and Greenberg DA (2004). Ischemia-induced neurogenesis is preserved but reduced in the aged rodent brain. Aging Cell 3, 373–377. [PubMed: 15569354]

Jin R, Yang G, and Li G (2010). Inflammatory mechanisms in ischemic stroke: role of inflammatory cells. J. Leukoc. Biol 87, 779–789. [PubMed: 20130219]

Kawano T, Anrather J, Zhou P, Park L, Wang G, Frys KA, Kunz A, Cho S, Orio M, and Iadecola C (2006). Prostaglandin E2 EP1 receptors: downstream effectors of COX-2 neurotoxicity. Nat. Med 12, 225–229. [PubMed: 16432513]

Liang Q, Luo Z, Zeng J, Chen W, Foo SS, Lee SA, Ge J, Wang S, Goldman SA, Zlokovic BV, et al. (2016). Zika virus NS4A and NS4B proteins deregulate Akt-mTOR signaling in human fetal neural stem cells to inhibit neurogenesis and induce autophagy. Cell Stem Cell 19, 663–671. [PubMed: 27524440]

Liao Y, Smyth GK, and Shi W (2014). featureCounts: an efficient general purpose program for assigning sequence reads to genomic features. Bioinformatics 30, 923–930. [PubMed: 24227677]

Liesz A, Suri-Payer E, Veltkamp C, Doerr H, Sommer C, Rivest S, Giese T, and Veltkamp R (2009). Regulatory T cells are key cerebroprotective immunomodulators in acute experimental stroke. Nat. Med 15, 192–199. [PubMed: 19169263]

Liesz A, Zhou W, Na SY, Hämmerling GJ, Garbi N, Karcher S, Mracsko E, Backs J, Rivest S, and Veltkamp R (2013). Boosting regulatory T cells limits neuroinflammation in permanent cortical stroke. J. Neurosci 33, 17350–17362. [PubMed: 24174668]

Liu F, Yuan R, Benashski SE, and McCullough LD (2009). Changes in experimental stroke outcome across the life span. J. Cereb. Blood Flow Metab 29, 792–802. [PubMed: 19223913]

Liu H, Wei X, Kong L, Liu X, Cheng L, Yan S, Zhang X, and Chen L (2015). NOD2 is involved in the inflammatory response after cerebral ischemia-reperfusion injury and triggers NADPH oxidase 2-derived reactive oxygen species. Int. J. Biol. Sci 11, 525–535. [PubMed: 25892960]

Lo EH, Moskowitz MA, and Jacobs TP (2005). Exciting, radical, suicidal: how brain cells die after stroke. Stroke 36, 189–192. [PubMed: 15637315]

Love MI, Huber W, and Anders S (2014). Moderated estimation of fold change and dispersion for RNA-seq data with DESeq2. Genome Biol. 15, 550. [PubMed: 25516281]

Markus TM, Tsai SY, Bollnow MR, Farrer RG, O'Brien TE, Kindler-Baumann DR, Rausch M, Rudin M, Wiessner C, Mir AK, et al. (2005). Recovery and brain reorganization after stroke in adult and aged rats. Ann. Neurol 58, 950–953. [PubMed: 16315284]

Mattson MP, and Camandola S (2001). NF-kappaB in neuronal plasticity and neurodegenerative disorders. J. Clin. Invest 107, 247–254. [PubMed: 11160145]

McGeer PL, and McGeer EG (2004). Inflammation and neurodegeneration in Parkinson's disease. Parkinsonism Relat. Disord 10 (Suppl 1), S3–S7. [PubMed: 15109580]

Mennicken F, Maki R, de Souza EB, and Quirion R (1999). Chemokines and chemokine receptors in the CNS: a possible role in neuroinflammation and patterning. Trends Pharmacol. Sci 20, 73–78. [PubMed: 10101968]

Menon S, Boyer NP, Winkle CC, McClain LM, Hanlin CC, Pandey D, Rothenfußer S, Taylor AM, and Gupton SL (2015). The E3 ubiquitin ligase TRIM9 is a filopodia off switch required for netrin-dependent axon guidance. Dev. Cell 35, 698–712. [PubMed: 26702829]

Morabito G, Giannelli SG, Ordazzo G, Bido S, Castoldi V, Indrigo M, Cabassi T, Cattaneo S, Luoni M, Cancellieri C, et al. (2017). AAV-PHP.B-mediated global-scale expression in the mouse nervous system enables GBA1 gene therapy for wide protection from synucleinopathy. Mol. Ther 25, 2727–2742. [PubMed: 28882452]

O'Collins VE, Macleod MR, Donnan GA, Horky LL, van der Worp BH, and Howells DW (2006). 1,026 experimental treatments in acute stroke. Ann. Neurol 59, 467–477. [PubMed: 16453316]

Obeso JA, Rodriguez-Oroz MC, Goetz CG, Marin C, Kordower JH, Rodriguez M, Hirsch EC, Farrer M, Schapira AH, and Halliday G (2010). Missing pieces in the Parkinson's disease puzzle. Nat. Med 16, 653–661. [PubMed: 20495568]

Ohtaki H, Nakamachi T, Dohi K, Aizawa Y, Takaki A, Hodoyama K, Yofu S, Hashimoto H, Shintani N, Baba A, et al. (2006). Pituitary adenylate cyclase-activating polypeptide (PACAP) decreases ischemic neuronal cell death in association with IL-6. Proc. Natl. Acad. Sci. USA 103, 7488–7493. [PubMed: 16651528]

Plooster M, Menon S, Winkle CC, Urbina FL, Monkiewicz C, Phend KD, Weinberg RJ, and Gupton SL (2017). TRIM9-dependent ubiquitination of DCC constrains kinase signaling, exocytosis, and axon branching. Mol. Biol. Cell 28, 2374–2385. [PubMed: 28701345]

Popa-Wagner A, Buga AM, and Kokaia Z (2011). Perturbed cellular response to brain injury during aging. Ageing Res. Rev 10, 71–79. [PubMed: 19900590]

Reischl S, Li L, Walkinshaw G, Flippin LA, Marti HH, and Kunze R (2014). Inhibition of HIF prolyl-4-hydroxylases by FG-4497 reduces brain tissue injury and edema formation during ischemic stroke. PLoS ONE 9, e84767. [PubMed: 24409307]

Rosen CL, Dinapoli VA, Nagamine T, and Crocco T (2005). Influence of age on stroke outcome following transient focal ischemia. J. Neurosurg 103, 687–694. [PubMed: 16266051]

Salminen A, Huuskonen J, Ojala J, Kauppinen A, Kaarniranta K, and Suuronen T (2008). Activation of innate immunity system during aging: NF-κB signaling is the molecular culprit of inflamm-aging. Ageing Res. Rev 7, 83–105. [PubMed: 17964225]

Sarabi AS, Shen H, Wang Y, Hoffer BJ, and Bäckman CM (2008). Gene expression patterns in mouse cortical penumbra after focal ischemic brain injury and reperfusion. J. Neurosci. Res 86, 2912–2924. [PubMed: 18506852]

Schwartz M, and Baruch K (2014). The resolution of neuroinflammation in neurodegeneration: leukocyte recruitment via the choroid plexus. EMBO J. 33, 7–22. [PubMed: 24357543]

Shapira S, Sapir M, Wengier A, Grauer E, and Kadar T (2002). Aging has a complex effect on a rat model of ischemic stroke. Brain Res. 925, 148–158. [PubMed: 11792363]

Shi M, Cho H, Inn KS, Yang A, Zhao Z, Liang Q, Versteeg GA, Amini-Bavil-Olyaee S, Wong LY, Zlokovic BV, et al. (2014). Negative regulation of NF-κB activity by brain-specific tripartite motif protein 9. Nat. Commun 5, 4820. [PubMed: 25190485]

Shichita T, Sugiyama Y, Ooboshi H, Sugimori H, Nakagawa R, Takada I, Iwaki T, Okada Y, Iida M, Cua DJ, et al. (2009). Pivotal role of cerebral interleukin-17-producing gammadeltaT cells in the delayed phase of ischemic brain injury. Nat. Med 15, 946–950. [PubMed: 19648929]

Shichita T, Hasegawa E, Kimura A, Morita R, Sakaguchi R, Takada I, Sekiya T, Ooboshi H, Kitazono T, Yanagawa T, et al. (2012). Peroxiredoxin family proteins are key initiators of post-ischemic inflammation in the brain. Nat. Med 18, 911–917. [PubMed: 22610280]

Shichita T, Ito M, Morita R, Komai K, Noguchi Y, Ooboshi H, Koshida R, Takahashi S, Kodama T, and Yoshimura A (2017). MAFB prevents excess inflammation after ischemic stroke by accelerating clearance of damage signals through MSR1. Nat. Med 23, 723–732. [PubMed: 28394332]

Simon A (2010). FastQC: a quality control tool for high throughput sequence data. http://www.bioinformaticsbabrahamacuk/projects/fastqc.

Stephenson D, Yin T, Smalstig EB, Hsu MA, Panetta J, Little S, and Clemens J (2000). Transcription factor nuclear factor-kappa B is activated in neurons after focal cerebral ischemia. J. Cereb. Blood Flow Metab 20, 592–603. [PubMed: 10724123]

Stowe AM, Wacker BK, Cravens PD, Perfater JL, Li MK, Hu R, Freie AB, Stüve O, and Gidday JM (2012). CCL2 upregulation triggers hypoxic preconditioning-induced protection from stroke. J. Neuroinflammation 9, 33. [PubMed: 22340958]

Strecker JK, Minnerup J, Gess B, Ringelstein EB, Schäbitz WR, and Schilling M (2011). Monocyte chemoattractant protein-1-deficiency impairs the expression of IL-6, IL-1β and G-CSF after transient focal ischemia in mice. PLoS ONE 6, e25863. [PubMed: 22031820]

Tanji K, Kamitani T, Mori F, Kakita A, Takahashi H, and Wakabayashi K (2010). TRIM9, a novel brain-specific E3 ubiquitin ligase, is repressed in the brain of Parkinson's disease and dementia with Lewy bodies. Neurobiol. Dis 38, 210–218. [PubMed: 20085810]

Wang Y, Kilic E, Kilic U, Weber B, Bassetti CL, Marti HH, and Hermann DM (2005). VEGF overexpression induces post-ischaemic neuroprotection, but facilitates haemodynamic steal phenomena. Brain 128, 52–63. [PubMed: 15509618]

Wang S, Chandler-Militello D, Lu G, Roy NS, Zielke A, Auvergne R, Stanwood N, Geschwind D, Coppola G, Nicolis SK, et al. (2010). Prospective identification, isolation, and profiling of a telomerase-expressing subpopulation of human neural stem cells, using sox2 enhancer-directed fluorescence-activated cell sorting. J. Neurosci 30, 14635–14648. [PubMed: 21048121]

Wang F, Flanagan J, Su N, Wang LC, Bui S, Nielson A, Wu X, Vo HT, Ma XJ, and Luo Y (2012a). RNAscope: a novel in situ RNA analysis platform for formalin-fixed, paraffin-embedded tissues. J. Mol. Diagn 14, 22–29. [PubMed: 22166544]

Wang Y, Zhang Z, Chow N, Davis TP, Griffin JH, Chopp M, and Zlokovic BV (2012b). An activated protein C analog with reduced anticoagulant activity extends the therapeutic window of tissue plasminogen activator for ischemic stroke in rodents. Stroke 43, 2444–2449. [PubMed: 22811462]

Wang Y, Zhao Z, Chow N, Rajput PS, Griffin JH, Lyden PD, and Zlokovic BV (2013). Activated protein C analog protects from ischemic stroke and extends the therapeutic window of tissue-type plasminogen activator in aged female mice and hypertensive rats. Stroke 44, 3529–3536. [PubMed: 24159062]

Wang Y, Zhao Z, Rege SV, Wang M, Si G, Zhou Y, Wang S, Griffin JH, Goldman SA, and Zlokovic BV (2016). 3K3A-activated protein C stimulates postischemic neuronal repair by human neural stem cells in mice. Nat. Med 22, 1050–1055. [PubMed: 27548576]

Wendeln AC, Degenhardt K, Kaurani L, Gertig M, Ulas T, Jain G, Wagner J, Häsler LM, Wild K, Skodras A, et al. (2018). Innate immune memory in the brain shapes neurological disease hallmarks. Nature 556, 332–338. [PubMed: 29643512]

Winkle CC, McClain LM, Valtschanoff JG, Park CS, Maglione C, and Gupton SL (2014). A novel Netrin-1-sensitive mechanism promotes local SNARE-mediated exocytosis during axon branching. J. Cell Biol 205, 217–232. [PubMed: 24778312]

Winkle CC, Hanlin CC, and Gupton SL (2016a). Utilizing combined methodologies to define the role of plasma membrane delivery during axon branching and neuronal morphogenesis. J. Vis. Exp 109, 53743.

Winkle CC, Olsen RH, Kim H, Moy SS, Song J, and Gupton SL (2016b). Trim9 deletion alters the morphogenesis of developing and adult-born hippocampal neurons and impairs spatial learning and memory.J. Neurosci 36, 4940–4958. [PubMed: 27147649]

Winkle CC, Taylor KL, Dent EW, Gallo G, Greif KF, and Gupton SL (2016c). Beyond the cytoskeleton: The emerging role of organelles and membrane remodeling in the regulation of axon collateral branches. Dev. Neurobiol 76, 1293–1307. [PubMed: 27112549]

Zhang G, Li J, Purkayastha S, Tang Y, Zhang H, Yin Y, Li B, Liu G, and Cai D (2013). Hypothalamic programming of systemic ageing involving IKK-β, NF-κB and GnRH. Nature 497, 211–216. [PubMed: 23636330]

Zhang Y, Chen K, Sloan SA, Bennett ML, Scholze AR, O'Keeffe S, Phatnani HP, Guarnieri P, Caneda C, Ruderisch N, et al. (2014). An RNA-sequencing transcriptome and splicing database of glia, neurons, and vascular cells of the cerebral cortex. J. Neurosci 34, 11929–11947. [PubMed: 25186741]

Highlights

- TRIM9 expression is increased in the peri-infarct area shortly after ischemic stroke
- *Trim9*-deficiency mice are more vulnerable to ischemia than wild-type mice
- AAV-mediated brain-wide TRIM9 expression ameliorates ischemic injury in mice

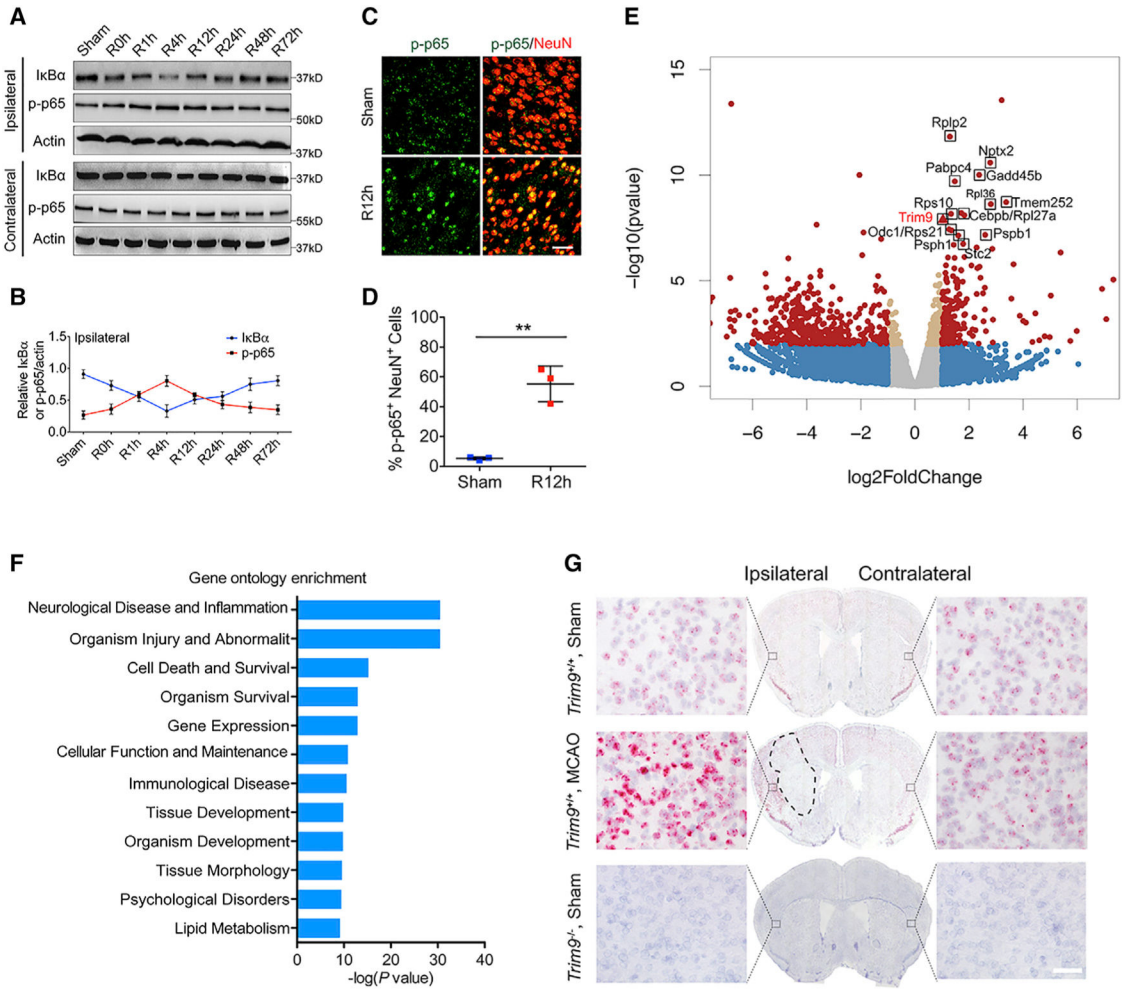

Figure 1. Upregulation of TRIM9 Expression in the Brains of MCAO Mice

(A and B) Representative immunoblots (A) and quantification (B) of IκBα degradation and NF-κB subunit p65 phosphorylation (p-p65) in tissue extracts of the ischemic brain hemispheres of 12-week-old C57BL/6J mice upon 30-min MCAO followed by various time points of reperfusion (R). Whole-tissue lysates were used for immunoblotting with antibodies against IκBα, p-p65, and actin. n = 3 mice per group.

(C and D) Representative confocal images (C) and quantifications (D) of p-p65 positive neurons (NeuN) in the infarct cortex of C57BL/6J mice 12 hr after 30-min MCAO. Scale bar, 20 μm. n = 3 mice per group. **p < 0.01 by Student's t test.

(E) Analysis of differential gene expression was based on RNA-seq and is presented as a volcano plot in the mouse ischemic hemispheres 12 hr after 30-min MCAO. Genes with over 2-fold expression changes are labeled blue and red. In this plot, the $-\log_{10}$ p value of each gene is plotted (on the vertical axis) against its $\log_2$ fold change (on the horizontal axis). Some of the top 20 upregulated genes based on adjusted p value are labeled in the black box on the right side. n = 2 mice in the sham group, and n = 3 mice in the MCAO group.

(F) Gene ontology enrichment analysis of the genes (plot based on $-\log_{10}$ p values for each pathway) in (E).

(G) *In situ* detection of *Trim9* mRNA using RNAscope probes on brain sections (at 0 mm from the bregma) of wild-type $Trim9^{+/+}$ mice 12 hr after 30-min MCAO or sham-operated littermates. Sham-operated $Trim9^{-/-}$ mice were included as controls. The closed dotted line indicates the infarct area. Scale bar, 50 mm. n = 3 mice per group.

Data in (B) and (C) are shown as mean ± SD.

See also Figure S1.

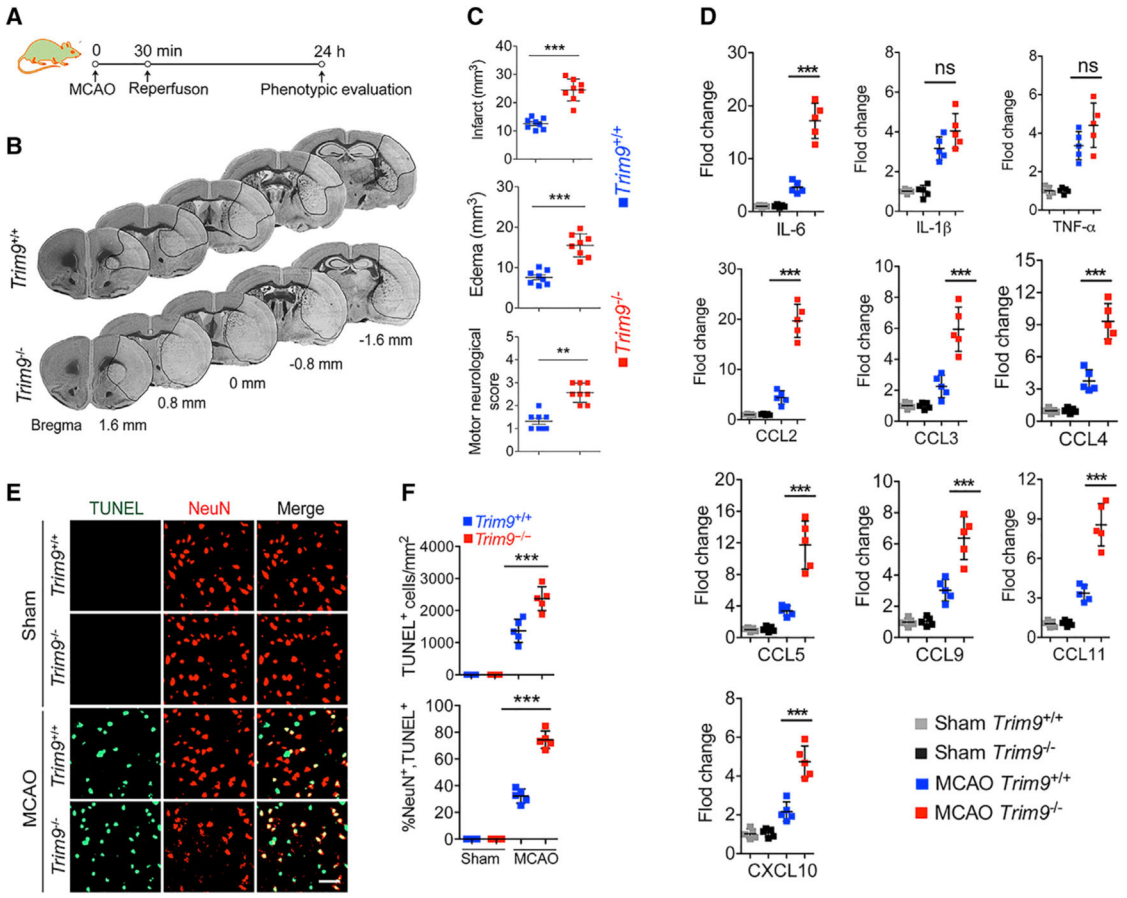

Figure 2. *Trim9* Deficiency Exacerbates Ischemic Brain Injury in Mice

(A) A diagram of the experimental procedures of ischemic stroke in mice.

(B) Representative cresyl violet staining images of the brain sections (at +1.6, +0.8, 0, −0.8, or −1.6 mm from the bregma) from *Trim9*$^{+/+}$ and *Trim9*$^{-/-}$ mice 24 hr after 30-min MCAO. The closed lines indicate infarct areas. n = 8 mice per group.

(C) Dot plots and quantifications of infarct volume, edema volume, and motor neurological scores of individual mouse from B. **p < 0.01 and ***p < 0.001 by Mann-Whitney *U* test.

(D) qRT-PCR analysis of a panel of inflammatory mediators in ischemic brain tissues of *Trim9*$^{+/+}$ and *Trim9*$^{-/-}$ mice 24 hr after 30-min MCAO. n = 5 mice per group. ***p < 0.001 by one-way ANOVA and Bonferroni's post hoc test. ns, non-significant.

(E and F) Representative confocal images (E) and quantification (F) of neuronal death based on a neural marker NeuN and TUNEL assay in the ischemic ipsilateral brain regions of *Trim9*$^{+/+}$ and *Trim9*$^{-/-}$ mice 24 hr after 30-min MCAO. TUNEL^{+} and NeuN^{+} and TUNEL^{+} indicate total number of cell death and neuronal cell death (%), respectively. Scale bar, 30 μm. n = 5 mice per group. ***p < 0.001 by Student's t test.

Data in (C), (D), and (F) are shown as mean ± SD.

See also Figures S2 and S3.

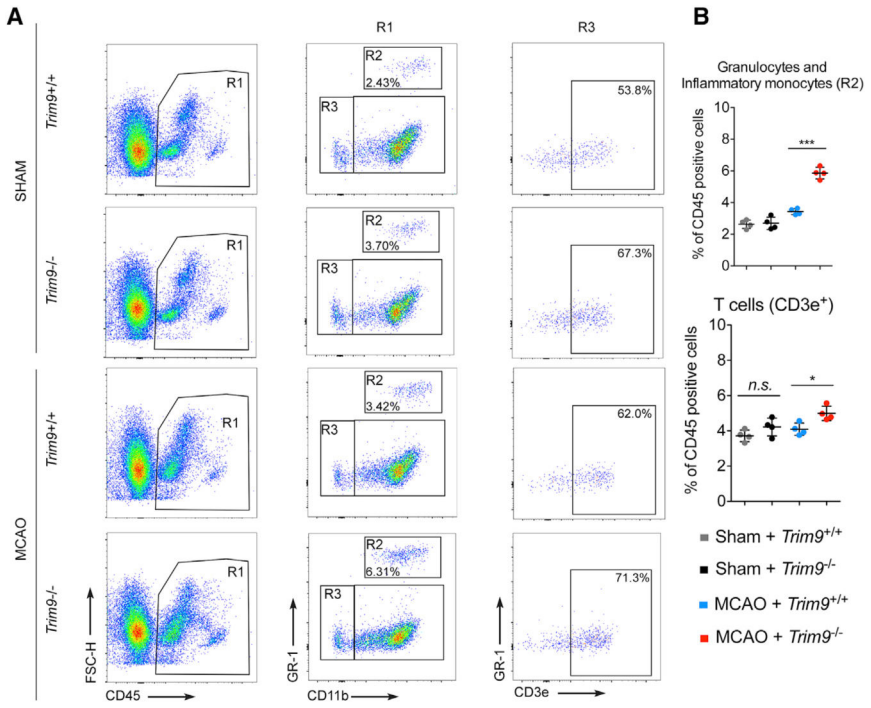

Figure 3. *Trim9* Deficiency Causes the In crease of Peripheral Immune Cell Infiltration in the Brain after Stroke

(A) Flow cytometry analysis of immune cells infiltrating into the ischemic hemisphere of *Trim9*$^{+/+}$ and *Trim9*$^{-/-}$ mice 24 hr after 30-min MCAO. The R1 population of CD45^{+} cells was selected and further gated for GR1^{+}CD11b^{+} granulocytes or inflammatory monocytes (R2) and CD11b^{-} lymphocytes (R3). The R3 population was further gated for CD3e^{+} T cells.

(B) Infiltrating immune cells. GR1^{+}CD11b^{+} granulocytes or inflammatory monocytes and CD3e^{+} T cells were presented as the percentage of CD45^{+} cells. n = 4 mice per group. *p < 0.05 and ***p <0.001 by one-way ANOVA and Bonferroni's post hoc test. Data are shown as mean ± SD.

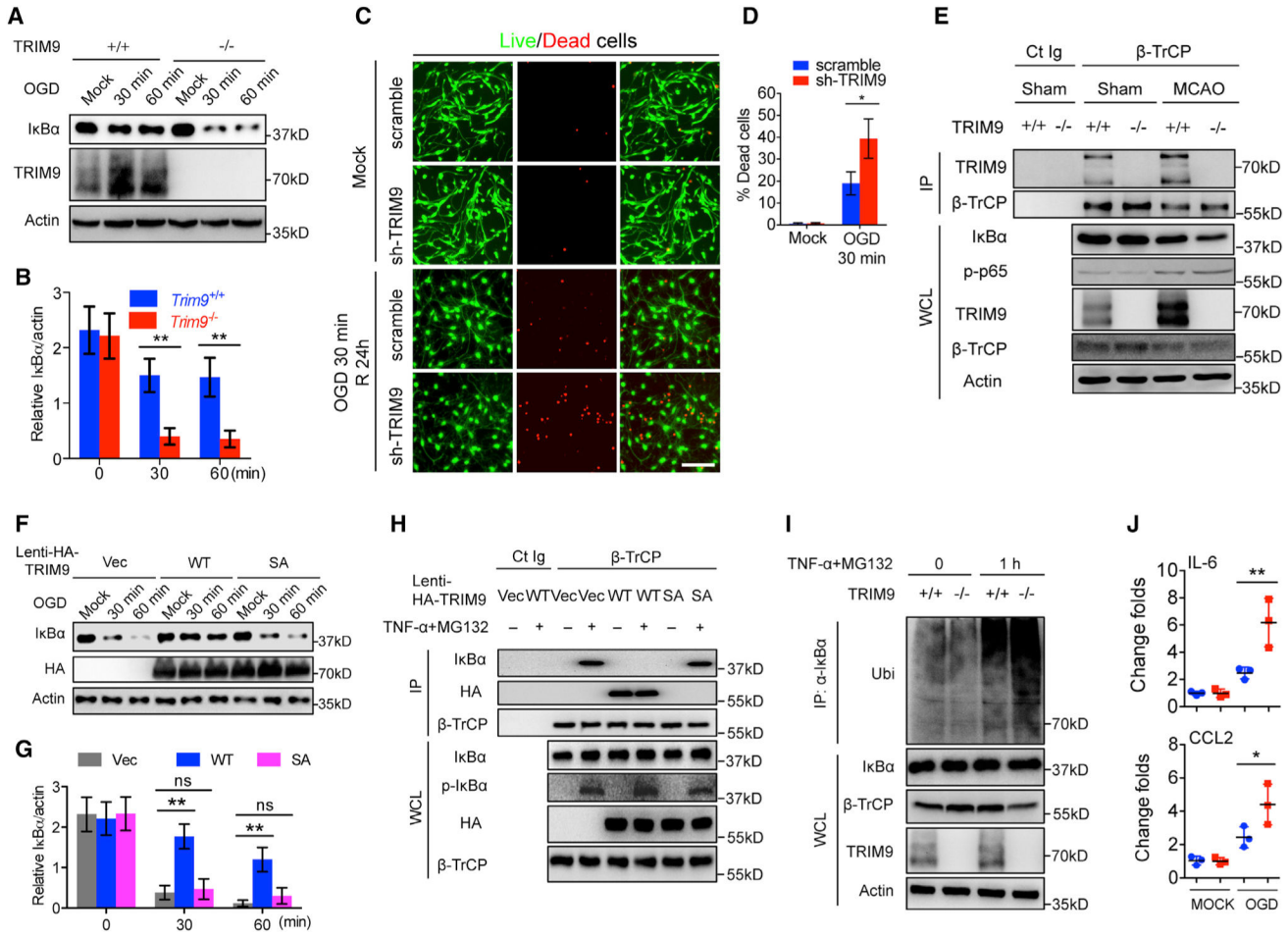

Figure 4. TRIM9 Suppresses NF-κB Signaling by Competing with IκBα for β-TrCP Interaction

(A and B) Representative immunoblots (A) and quantification (B) of IκBα in primary cortical neurons isolated from *Trim9*$^{+/+}$ and *Trim9*$^{-/-}$ embryos stimulated by 30 or 60 min of oxygen-glucose deprivation (OGD) followed by reoxygenation (R24h). Whole-cell lysates (WCLs) were used for immunoblotting with anti-TRIM9 and anti-actin antibody. **p < 0.01 by Student's t test.

(C and D) Representative images (C) and quantification (D) of Live-Dead viability assays 24 hr after 30-min OGD stimulation of human neural progenitor cell (hNPC)-derived neurons transduced with scramble or TRIM9-specific shRNA lentivirus. Scale bar, 30 μm.

(E) Representative immunoblots of the β-TrCP-TRIM9 interaction. Ischemic brain tissues of *Trim9*$^{+/+}$ and *Trim9*$^{-/-}$ mice 24 hr after 30-min MCAO were used for immunoprecipitation (IP) with anti-β-TrCP, followed by immunoblotting (IB) with anti-β-TrCP or anti-TRIM9. WCLs were also used for IB with various antibodies. Ct Ig, isotype control immunoglobulin.

(F and G) Representative immunoblot (F) and quantification (G) of IκBα in *Trim9*$^{-/-}$ primary neurons transduced with lentivirus carrying vector (Vec), mouse hemagglutinin (HA)-TRIM9 wild-type (WT), or HA-TRIM9 SA mutant 24 hr after 30- or 60-min OGD. **p < 0.01 by Student's t test. ns, non-significant.

(H and I) Comparison between the β-TrCP-TRIM9 interaction and the β-TrCP-IκBα interaction (H) and IκBα ubiquitination (I). *Trim9*$^{-/-}$ primary neurons transduced with Vec,

TRIM9 WT, or TRIM9 SA mutant lentivirus were stimulated with mock (−) or TNF-α (25 ng/ml) + MG312 (10 μM) (+) for 1 hr (see STAR Methods for details). WCLs were used for IP with anti-β-TrCP, followed by IB with anti-IκBα or anti-HA (H) or for IP with anti-IκBα, followed by IB with anti-ubiquitin antibody (I). WCLs were also used for IB with antibodies against IκBα, p-IκBα, HA, β-TrCP, TRIM9, or actin.

(J) qRT-PCR analysis of a panel of inflammatory mediators, including IL-6 and CCL2, in *Trim9*$^{+/+}$ (blue) and *Trim9*$^{-/-}$ (red) primary neurons primary neurons 24 hr after 30-min OGD treatment. **$p < 0.01$ and *$p < 0.05$ by one-way ANOVA and Bonferroni's post hoc test.

Data in (B), (D), (G), and (J) are from three independent experiments, shown as mean ± SD. See also Figures S4 and S5.

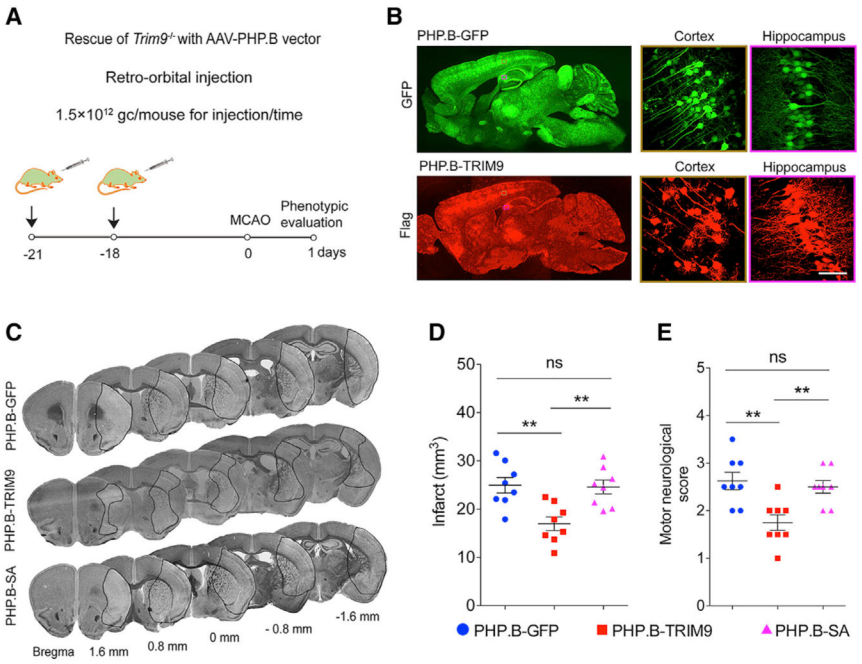

Figure 5. Noninvasive AAV-PHP.B-Mediated Brain-wide TRIM9 Expression Alleviates Ischemic Injury in *Trim9*$^{-/-}$ Mice

(A) A diagram of the experimental design. *Trim9*$^{-/-}$ mice were retro-orbital injected twice with 1.5 × 10^{12} genome copy of recombinant AAV vector, including AAV-PHP.B:CAG-GFP (PHP.B-GFP), AAV-PHP.B:CAG-FLAG-TRIM9 (PHP.B-TRIM9), and AAV-PHP.B:CAG-FLAG-TRIM9-SA (PHP.BSA). These mice were tested 21 days or 18 days prior to MCAO conditions.

(B) Representative images of GFP and FLAG-TRIM9 expression in brain sections 21 days post-infection of recombinant AAV. Scale bar, 50 μm. n = 3 mice per group.

(C) Representative cresyl violet staining images of the brain sections (at +1.6, +0.8, 0, −0.8, or −1.6 mm from the bregma) of recombinant AAV-infected *Trim9*$^{-/-}$ mice that were tested 24 hr after 30-min MCAO. The area within the closed line indicates injured tissue. Scale bar, 30 μm. n = 8 mice per group.

(D and E) Quantification of infarct volume (D) and motor neurological scores (E) of individual mice described in (C). **p < 0.01 by one-way ANOVA and Tukey's post hoc test. ns, non-significant. Data are shown as mean ± SD.

See also Figure S6.

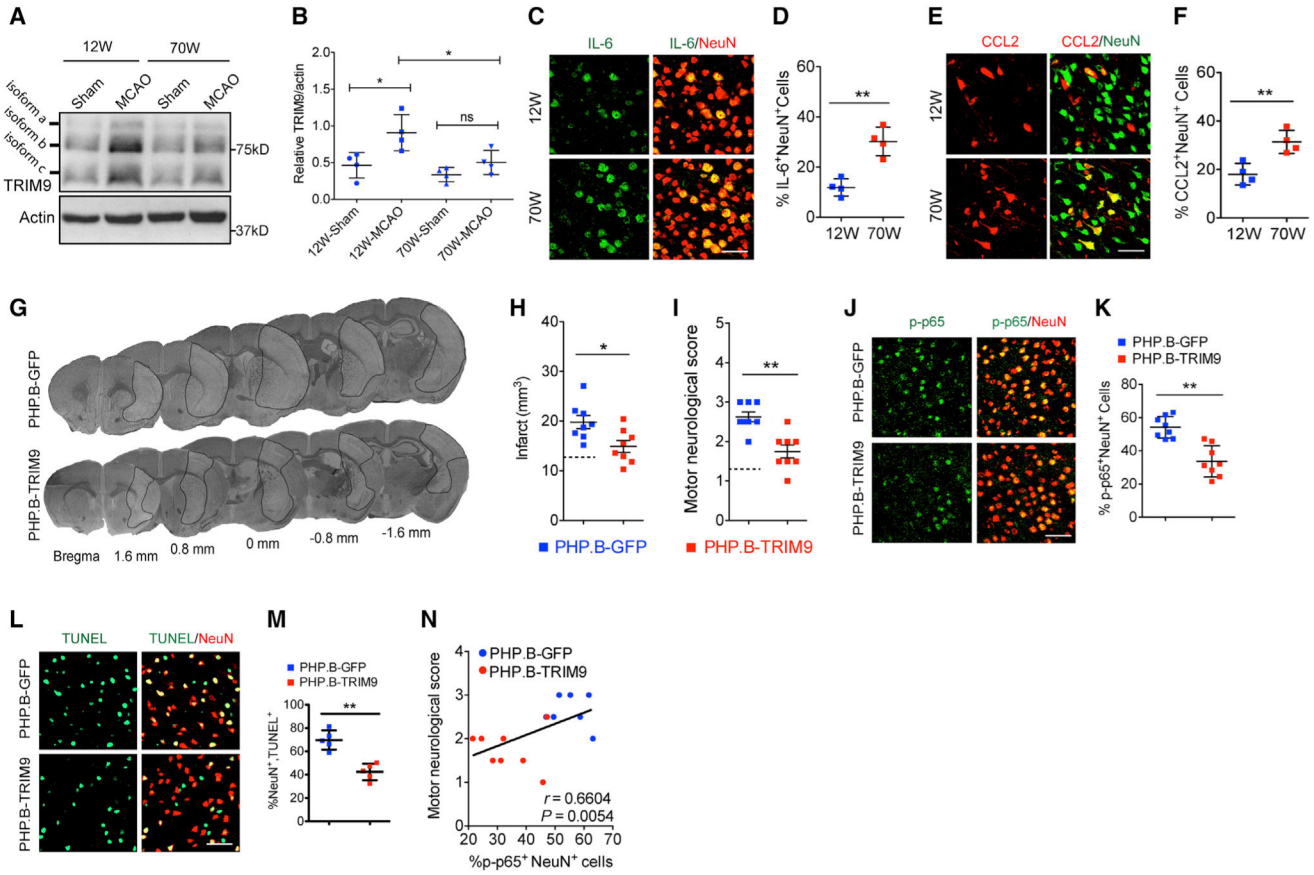

Figure 6. AAV-PHP.B-Mediated Brain-wide TRIM9 Expression Ameliorates Ischemic Injury in C57BL/6J Middle-Aged Mice

(A and B) Representative immunoblots (A) and quantification (B) of TRIM9 in brain tissue extracts of the ischemic brain hemispheres of C57BL/6J young or aged mice upon 30-min MCAO, followed by 12-hr reperfusion. Whole-tissue lysates were used for immunoblotting with antibodies against TRIM9 and actin. Isoform b was used for quantification. n = 4 mice per group. *p < 0.05 by one-way ANOVA and Bonferroni's post hoc test. ns, non-significant.

(C–F) Representative confocal images and quantifications of IL-6-positive (C and D) and CCL2-positive (E and F) neurons (NeuN) in the ischemic ipsilateral cortex regions of 12-week-old (12W) and 70-week-old (70W) C57BL/6J mice 12 hr after 30-min MCAO. Scale bar, 30 μm. n = 4 mice per group. **p < 0.01 by Student's t test.

(G) Representative cresyl violet staining images of the brain sections (at +1.6, +0.8, 0, −0.8, or −1.6 mm from the bregma) of recombinant AAV-infected aging mice that were tested 24 hr after 30-min MCAO. The area within the closed line indicates injured tissue. Scale bar, 30 μm. n = 8 mice per group.

(H and I) Quantification of infarct volume (H) and motor neurological scores (I) of individual mice described in (G). The dashed line indicates the mean value from *Trim9*$^{+/+}$ mice in Figure 2c. *p < 0.05 and **p < 0.01 by Mann-Whitney *U* test. ns, non-significant.

(J and K) Representative confocal images (J) and quantification (K) of p-p65-positive neuronal cells in the peri-infarct regions of ischemic brain of recombinant AAV-infected

aging mice 24 hr after 30-min MCAO. Scale bar, 30 μm. n = 8 mice per group. **p < 0.01 by Mann-Whitney *U* test.

(L and M) Representative confocal images (L) and quantifications (M) of neuronal death based on a TUNEL assay in the infarct region of ischemic brain of aging mice injected with the indicated AAV 24 hr after 30-min MCAO. Scale bar, 30 mm. n = 5 mice per group. **p < 0.01 by Mann-Whitney *U* test.

(N) Correlation between the p-p65-positive neuron population level and the motor neurological behavior score in PHP.B-GFP- or PHP.B-TRIM9-infected aged mice 24 hr after 30-min MCAO.

Data in (B), (D), (F), (H), (I), (K), (M), and (N) are shown as mean ± SD.

KEY RESOURCES TABLE

REAGENT or RESOURCE	SOURCE	IDENTIFIER
Antibodies		
Mouse monoclonal anti-IκBα	Cell Signaling Technology	Cat #9247
Rabbit monoclonal anti-pIκBα	Cell Signaling Technology	Cat #2859
Rabbit monoclonal anti-p-p65	Cell Signaling Technology	Cat #3033
Mouse monoclonal anti-β-actin	Santa Cruz	Cat #sc-47778
Rabbit polyclonal anti-TRIM9	Stephanie L. Gupton lab	N/A
Mouse monoclonal anti-ubiquitin	Santa Cruz	Cat #sc-8017
Rabbit monoclonal anti-β-TrCP	Cell Signaling Technology	Cat #4394
Mouse monoclonal anti-HA	Santa Cruz	Cat #sc-57594
Mouse monoclonal anti-GFP	Santa Cruz	Cat #sc-101525
Mouse monoclonal anti-Flag	Sigma	Cat #F1804
Mouse monoclonal anti-GFAP	Cell Signaling Technology	Cat #3670
Rabbit monoclonal anti-Iba1	Abeam	Cat #ab178846
Rabbit polyclonal anti-NeuN	Millipore	Cat #ABN78
Mouse monoclonal anti-SMI312	Abeam	Cat #ab24574
Rabbit polyclonal anti-NG2	Abeam	Cat #ab83178
Mouse monoclonal anti-Olig2	Millipore	Cat #MABN50
Rat monoclonal anti-IL6	Thermo	Cat #AMC0864
Mouse monoclonal anti-NeuN	Millipore	Cat #MAB377
Rabbit polyclonal anti-CCL2	Abeam	Cat #9779
Mouse monoclonal anti-MAP2	Abeam	Cat #ab11267
Rat anti-CD45	BD PharMingen	Cat #103116
Rat anti-CD11b	eBioscience	Cat #48-0112-82
Rat anti-GR1	BD PharMingen	Cat #108412
Rat anti-CD3e	BD PharMingen	Cat #100328
Rat anti-CD11c	BD PharMingen	Cat #117318
Chemicals, Peptides, and Recombinant Proteins		
Protease inhibitor cocktail	Roche	Cat #4693159001
Phosphatase inhibitor PhosSTOP	Roche	Cat #4906845001
Recombinant mouse TNF-α	Biolegend	Cat #575202
Recombinant mouse IL-1β	Biolegend	Cat #575102
MG132	R&D Systems	Cat #1748
Critical Commercial Assays		
RNeasy Mini Kit	QIAGEN	Cat #74104
KAPA stranded mRNA-seq Kit	KAPA Biosystems	Cat #kk8421
iScript cDNA Synthesis Kit	Bio-Rad	Cat #1708891
iQ SYBR Green supermix	Bio-Rad	Cat #1708880

REAGENT or RESOURCE	SOURCE	IDENTIFIER
RNAscope 2.5 HD Reagent Kit-RED	Advanced Cell Diognostics	Cat #322360
Cresyl Echt Violet Staining Kit	American MasterTech	Cat #AHC0443
In Situ Cell Death Detection Kit	Roche	Cat #11684795910
In Situ Cell Death Detection Kit	Roche	Cat #12156792910
Mouse IL-6 ELISA Kit	BD Biosciences	Cat #555240
Mouse IL-1β ELISA Kit	BD Biosciences	Cat #559603
Mouse TNF-α ELISA Kit	BD Biosciences	Cat #555268
Mouse IL-10 ELISA Kit	BD Biosciences	Cat #555252
Neural Tissue Dissociation Kit	MACA Miltenyl Biotec	Cat #130093231
BCA Protein Assay Kit	Thermo Fisher Scientific	Cat #23227
Lipofectamine 2000 Transfection Kit	Thermo Fisher Scientific	Cat #11668027
Lipofectamine RNAiMAX Kit	Thermo Fisher Scientific	Cat #13778075
LIVE-DEAD Viiability /Cytotoxicity Kit	Thermo Fisher Scientific	Cat #L3224
Propidium iodide	Invitrogen	Cat #P3566
Deposited Data		
RNA-seq data	This paper	GEO: GSE114652
Experimental Models: Cell Lines		
HEK293T	ATCC	Cat #CRL-11268
Trim9-knockout neurons	This paper	N/A
7r/m9-knockout MEFs	This paper	N/A
Trim9-derived neurons	This paper	N/A
Experimental Models: Organisms/Strains		
C57BL/6J mice	The Jackson Laboratory	JAX stock 000664
Trim9 deficient (*Trim9*$^{+/-}$) mice	Stephanie L Gupton lab	N/A
Oligonuoleotides		
Primers for RT-qPCR (See Table S3)		N/A
RNAscope Probe: Murine *Trim9*-specific probe	Advanced Cell Diagnostics	Cat #479071
Recombinant DNA		
Plasmid: pCDH-HA-*Trim9*	This paper	N/A
Plasmid: pCDH-HA-*Trim9*-SA	This paper	N/A
Plasmid: AAV-PHP.B vector	Viviana Gradinaru lab	N/A
Plasmid: AAV-PHP.B:CAG-GFP	This paper	N/A
Plasmid: AAV-PHP.B:CAG-*Trim9*	This paper	N/A
Plasmid: AAV-PHP.B:CAG-*Trim9*-SA	This paper	N/A
Software and Algorithms		
GraphPad Prism v6.03	GraphPad Software	https://www.graphpad.com/